Since January 2020 Elsevier has created a COVID-19 resource centre with free information in English and Mandarin on the novel coronavirus COVID-19. The COVID-19 resource centre is hosted on Elsevier Connect, the company's public news and information website.

Nano Today 38 (2021) 101136

Contents lists available at ScienceDirect

Nano Today

journal homepage: www.elsevier.com/locate/nanotoday

2D MXenes with antiviral and immunomodulatory properties: A pilot study against SARS-CoV-2

Mehmet Altay Unal[a,1], Fatma Bayrakdar[b,1], Laura Fusco[c,d,1], Omur Besbinar[a,e], Christopher E. Shuck[f], Süleyman Yalcin[b], Mine Turktas Erken[g], Aykut Ozkul[h,s], Cansu Gurcan[a,e], Oguzhan Panatli[e], Gokce Yagmur Summak[a], Cemile Gokce[e], Marco Orecchioni[i], Arianna Gazzi[c,j], Flavia Vitale[k], Julia Somers[l], Emek Demir[l], Serap Suzuk Yildiz[b], Hasan Nazir[m], Jean-Charles Grivel[n], Davide Bedognetti[d,o,p], Andrea Crisanti[q], Kamil Can Akcali[a,r], Yury Gogotsi[f,*], Lucia Gemma Delogu[c,*], Açelya Yilmazer[a,e,**]

[a] Stem Cell Institute, Ankara University, Balgat, Ankara, Turkey
[b] Ministry of Health General Directorate of Public Health, Microbiology References Laboratory, Ankara, Turkey
[c] Department of Biomedical Sciences, University of Padua, Padua, Italy
[d] Cancer Research Department, Sidra Medicine, Doha, Qatar
[e] Department of Biomedical Engineering, Ankara University, Golbasi, Ankara, Turkey
[f] A.J. Drexel Nanomaterials Institute and Department of Materials Science and Engineering, Drexel University, Philadelphia, PA, USA
[g] Department of Biology, Gazi University, Ankara, Turkey
[h] Department of Virology, Faculty of Veterinary Medicine, Ankara University, Ankara, Turkey
[i] La Jolla Institute for Immunology, La Jolla, CA, USA
[j] Department of Chemical and Pharmaceutical Sciences, University of Trieste, Trieste, Italy
[k] Department of Neurology, Bioengineering, Physical Medicine & Rehabilitation, Center for Neuroengineering and Therapeutics, University of Pennsylvania, Philadelphia, PA, USA
[l] Oregon Health & Sciences University, Department of Molecular and Medical Genetics, Portland, OR, USA
[m] Department of Chemistry, Ankara University, Tandogan, Ankara, Turkey
[n] Deep Phenotyping Core, Sidra Medicine, Doha, Qatar
[o] Department of Internal Medicine and Medical Specialties (DiMI), University of Genoa, Genoa, Italy
[p] College of Health and Life Sciences, Hamad Bin Khalifa University, Doha, Qatar
[q] Department of Molecular Medicine, Padua University Hospital, Padua, Italy
[r] Department of Biophysics, Faculty of Medicine, Ankara University, Ankara, Turkey
[s] Biotechnology Institute, Ankara University, Ankara, Turkey

ARTICLE INFO

Article history:
Received 5 January 2021
Received in revised form 22 February 2021
Accepted 15 March 2021
Available online 18 March 2021

Keywords:
MXene
Toxicity
Immune system
Antiviral properties

ABSTRACT

Two-dimensional transition metal carbides/carbonitrides known as MXenes are rapidly growing as multimodal nanoplatforms in biomedicine. Here, taking SARS-CoV-2 as a model, we explored the antiviral properties and immune-profile of a large panel of four highly stable and well-characterized MXenes - $Ti_3C_2T_x$, $Ta_4C_3T_x$, $Mo_2Ti_2C_3T_x$ and $Nb_4C_3T_x$. To start with antiviral assessment, we first selected and deeply analyzed four different SARS-CoV-2 genotypes, common in most countries and carrying the wild type or mutated spike protein. When inhibition of the viral infection was tested in vitro with four viral clades, $Ti_3C_2T_x$ in particular, was able to significantly reduce infection only in SARS-CoV-2/clade GR infected Vero E6 cells. This difference in the antiviral activity, among the four viral particles tested, highlights the importance of considering the viral genotypes and mutations while testing antiviral activity of potential drugs and nanomaterials. Among the other MXenes tested, $Mo_2Ti_2C_3T_x$ also showed antiviral properties.

* Corresponding authors.
** Corresponding author at: Department of Biomedical Engineering, Ankara University, Golbasi, Ankara, Turkey.
E-mail addresses: gogotsi@drexel.edu (Y. Gogotsi), luciagemma.delogu@unipd.it (L.G. Delogu), ayilmazer@ankara.edu.tr (A. Yilmazer).
[1] Equal contribution.

https://doi.org/10.1016/j.nantod.2021.101136

Viral clades
Nanomedicine
Single cell mass cytometry

Proteomic, functional annotation analysis and comparison to the already published SARS-CoV-2 protein interaction map revealed that MXene-treatment exerts specific inhibitory mechanisms. Envisaging future antiviral MXene-based drug nano-formulations and considering the central importance of the immune response to viral infections, the immune impact of MXenes was evaluated on human primary immune cells by flow cytometry and single-cell mass cytometry on 17 distinct immune subpopulations. Moreover, 40 secreted cytokines were analyzed by Luminex technology. MXene immune profiling revealed i) the excellent bio and immune compatibility of the material, as well as the ability of MXene ii) to inhibit monocytes and iii) to reduce the release of pro-inflammatory cytokines, suggesting an anti-inflammatory effect elicited by MXene. We here report a selection of MXenes and viral SARS-CoV-2 genotypes/mutations, a series of the computational, structural and molecular data depicting deeply the SARS-CoV-2 mechanism of inhibition, as well as high dimensional single-cell immune-MXene profiling. Taken together, our results provide a compendium of knowledge for new developments of MXene-based multi-functioning nanosystems as antivirals and immune-modulators.

Introduction

From the very beginning of the coronavirus disease 2019 (COVID-19) pandemic, caused by the novel SARS-CoV-2, scientists with diverse backgrounds have converged in an effort to deal with this emergency [1–3]. In addition to extensive pre-clinical and clinical trials carried out for the design of drugs and vaccines, various research efforts are being conducted to achieve better viral inactivation strategies outside the patients, such as the development of self-disinfecting surfaces or personal protective equipment (PPE). In this view, we and others have recently highlighted how nanotechnology and 2D nanomaterials can offer new approaches to cope with the COVID-19 pandemic and infectious diseases in general, including future pandemics [4–17]. The fact that lipid nanoparticle-based vaccines have already obtained approval by the US Food and Drug Administration and European Medical Agency shows that expertise and knowledge developed in the field of nanomedicine has enabled nanoparticle-based vaccine trials to take place in the fight against COVID-19 [18–21]. Therefore, research to advance our understanding of nanomaterial behavior in biological systems is crucial to tackle any future life-threatening disease.

The rational design of nanomaterials, characterized by specific physicochemical properties, turns them into active platforms endowed with different activities exploitable in biomedicine [4,22–24]. In particular, two-dimensional (2D) nanomaterials have been investigated for a wide range of biomedical applications, including cancer theranostics, biosensors and antimicrobial platforms [25–29]. In 2011, the novel class of 2D materials was discovered; transition metal carbides/nitrides (MXenes) [30,31]. Since then, more than 30 stoichiometric members of this family have been successfully synthetized, along with tunable solid-solution MXenes, and more than 100 other forms of MXenes have been predicted *in silico* [32–34]. MXenes have the general formula $M_{n+1}X_nT_x$, where M is an early transition metal (Ti, Nb, V, etc.), X is C and/or N, n is 1–4, and T_x represents the surface terminations (typically, O, OH, F, and Cl) [33]. Due to their wet chemical etching route and surface terminations, MXenes are natively hydrophilic and negatively charged [35–37]. In particular – and almost unique among other 2D nanomaterials - the hydrophilic nature allows to easily integrate MXenes within common biomedical platforms without the need of any specific functionalization or surfactant.

It has been reported that 2D materials can show antimicrobial activity against bacteria, virus, and fungi [25,38–40]. For instance, numerous studies evaluated the antibacterial effectiveness of various graphene-based materials (GBMs), with different lateral size, thickness, functionalization and conjugation to polymers or metal nanoparticles [25], delineating the underlying mechanisms behind this activity (e.g., oxidative stress, inhibition of electron transports, direct contact with bacteria membrane and mechanical damage) [41–43]. To date, there have been numerous studies conducted on MXenes, showing their potential for a number of biomedical applications, including antibacterial properties [39,44–53], as we previously demonstrated for $Ti_3C_2T_x$ [49–51,54]. In addition to antibacterial activity, a few studies have demonstrated the potential application of 2D materials as antivirals [52,53,55–57]. However, no study so far has explored the antiviral activity of MXenes. Therefore, considering the intrinsic properties of MXenes and encouraged by our previous finding on their potential applications in the antimicrobial field, here we explore an in-depth antiviral behavior against four different SARS-CoV-2 genotypes on a large panel of MXenes in four different forms.

Moreover, in order to use any 2D material for biomedical applications, their biocompatibility and toxicity profile should be clearly and thoroughly assessed in order to envisage their potential applications [26,27]. Any exposure to these nanomaterials will result in immediate recognition by immune cells, the body's first line of defense against exogenous agents [58,59]. In this context, as we recently introduced by the nanoimmunity-by-design concept, the specific nanomaterial physicochemical properties can dictate their reactivity and interactions with immune cells [23]. This makes the assessment of the health and safety risks a challenging field, hampering their implementation into biomedical applications [23,60,61]. Moreover, the immune system reaction and cytokine storm syndrome are important factors in the progression of COVID-19 and as well as in other disease. It is therefore urgent to dissect the immune impact of MXene to foster its full potential. None of the studies present in literature reports a deep immune profile of MXenes at the single-cell level. In this study, simultaneously with its antiviral activity, we fully explored the immune cell compatibility of MXenes.

In this study, following material synthesis and characterization, we performed detailed antiviral and deep-immune profiling experimentation (Fig. 1A). We first delineated the antiviral activity simultaneously of four different highly stable MXenes: $Ti_3C_2T_x$, $Ta_4C_3T_x$, $Mo_2Ti_2C_3T_x$ and $Nb_4C_3T_x$. We selected four viral genotypes from the viral repository of the Microbiology References Laboratory in Turkey. We then assessed the viral inhibition by quantification of viral copy numbers and viability of Vero E6 cells. Based on this, we performed *in silico* molecular docking and proteomic analysis to reveal the mechanism of viral inhibition. Finally, because each immune subpopulation can play a different role with possible reactions to MXene-based clinical nanomedicine, we performed viability, activation assay by flow cytometry and a wide analysis on cytokine, chemokines production by Luminex. An in-depth analysis at the single-cell level towards 17 primary human immune cell subpopulations was then performed by single-cell mass cytometry looking at the impact on viability and their functionality by cytokine production.

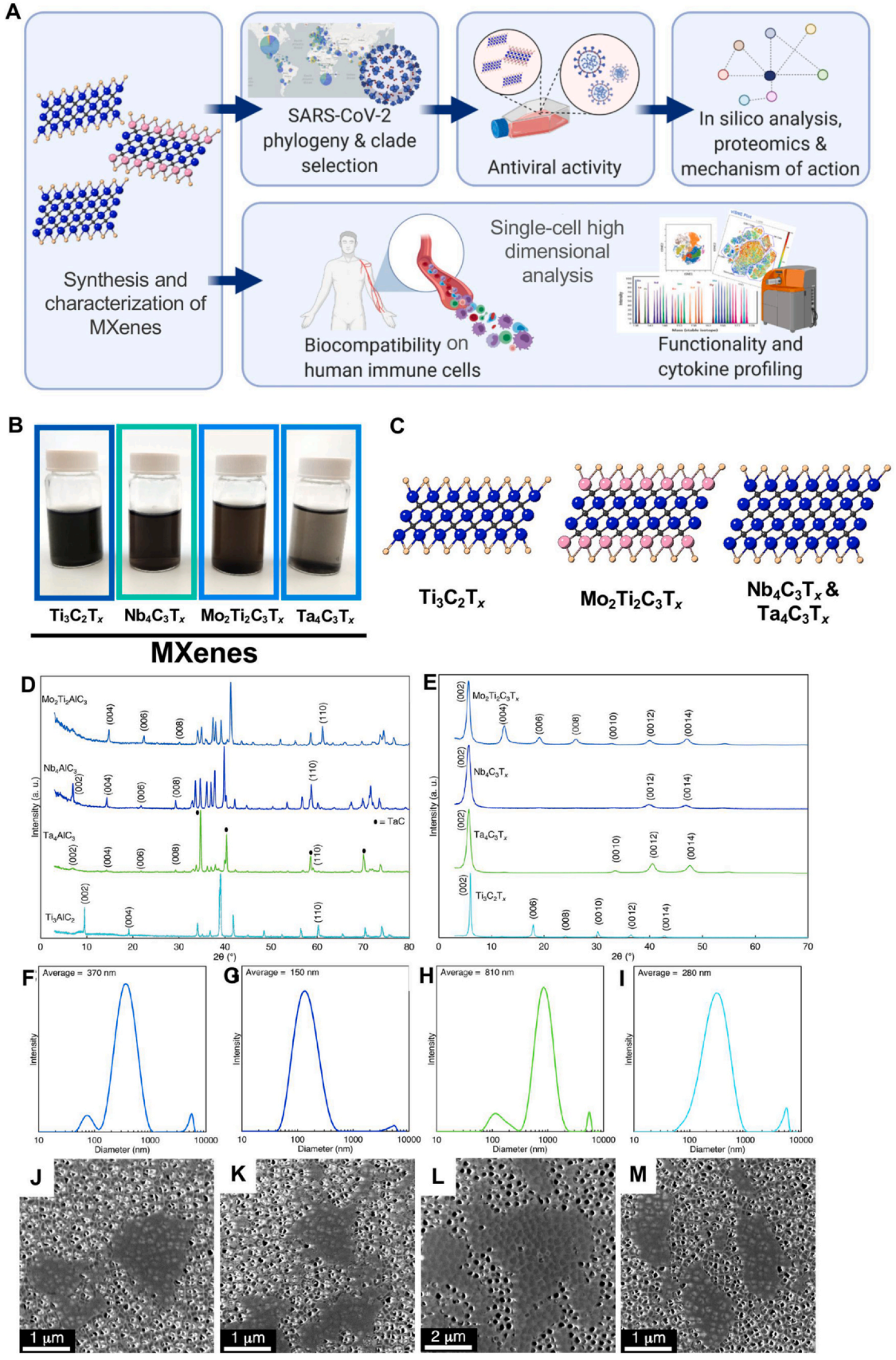

Fig. 1. Study design and material characterization. A) Overview of the study design. B) Images of aqueous suspensions of MXene C) Crystal structure of the 2D materials. $Ti_3C_2T_x$: Ti (blue), T_x (O, OH, F) (brown), C (grey); $Mo_2Ti_2C_3T_x$; Mo (pink), Ti (blue) T_x (brown), C (grey); $Nb_4C_3T_x$ and $Ta_4C_3T_x$: Ti (blue), T_x (brown), C (grey). D) X-ray diffraction (XRD) patterns of the MAX phase precursors used for synthesis of the MXenes. E) XRD patterns of vacuum-filtered MXene films after synthesis. Dynamic light scattering (DLS) of F) $Mo_2Ti_2C_3T_x$, G) $Nb_4C_3T_x$, H) $Ta_4C_3T_x$, and I) $Ti_3C_2T_x$ showing the flake size distributions of the MXenes used in this study. Scanning electron microscopy (SEM) images of J) $Mo_2Ti_2C_3T_x$, K) $Nb_4C_3T_x$, L) $Ta_4C_3T_x$, and M) $Ti_3C_2T_x$ MXenes used in this study.

Results

To start with, MXenes (Fig. 1B, C) were produced by selectively etching Al from MAX phases (details in SI). X-ray diffraction (XRD) patterns of the precursor MAX powders (Ti_3AlC_2, Nb_4AlC_3, $Mo_2Ti_2AlC_3$, and Ta_4AlC_3) and delaminated MXenes ($Ti_3C_2T_x$, $Nb_4C_3T_x$, $Mo_2Ti_2C_3T_x$, and $Ta_4C_3T_x$) are shown in Fig. 1D, E respectively. The MAX phases have p63/mmc space group, with the (00*l*) and (110) peaks labeled. For Ti_3AlC_2, the (002) peak is located at 9.54° (9.26 Å), and after etching and delamination with tetramethylammonium hydroxide (TMAOH), the peak shifts to 5.94° (14.78 Å) for $Ti_3C_2T_x$. Similar trends are observed for the other MAX to MXene conversions, indicating successful removal of the Al layers for all MXenes studied here. In the MXene XRD patterns, only the (00*l*) peaks remain, indicating successful etching and delamination, with no impurities remaining in the MXene colloid [62]. Dynamic light scattering (DLS; Fig. 1F-I) was used to characterize the average flake size in the MXene colloids, indicating that the $Ti_3C_2T_x$ flakes were on average 280 nm, with flakes up to 1 µm in size; $Mo_2Ti_2C_3T_x$, $Nb_4C_3T_x$, and $Ta_4C_3T_x$ had average flake sizes of 370, 150, and 810 nm, respectively. Scanning electron microscopy (SEM; Fig. 1J-M) was used to confirm successful delamination of the MXene flakes. From the representative image, the flakes used in this study are confirmed to be single layers (about 1 nm in thickness), with sizes commensurate with DLS. They have O, OH and F on the surface, which affect their chemical properties and biological activity [62–64].

The Global Initiative on Sharing All Influenza Data (GISAID) platform was established in 2008 in order to offer data sharing mechanism for influenza researchers, scientists and health officials to share all influenza genetic and related data. Following the emergence of SARS-CoV-2 in December 2019, GISAID started to share genomes deposited from all around the world (Fig. 2A) which also led to the introduction of a nomenclature system for major clades, based on marker mutations (https://www.gisaid.org) in reference to the complete genome of the first isolate from Wuhan [65]. Currently, the platform classifies SARS-CoV-2 genomes into 8 clades and among which GR, GH and S clades have been identified in most of the countries, whereas the genomes from the clade designated as other is more specific to locations (Fig. 2A). The viral particles used in this study were obtained from the repository of the Microbiology Reference Laboratory in Turkey and all the genomes have been previously sequenced and classified by GISAID (Fig. 2B and C). In order to cover a wider range of SARS-CoV-2 genotypes present in most countries and carrying wild type or mutated viral proteins, we have selected 4 clades (GR, GH, S and other) to test in this study. Especially the mutations such as D614G on the spike have been reported to be very important in viral infectivity [66–69]. Mutations arising in different countries take the attention of all human beings, but especially more for scientists working to develop drugs or vaccines against SARS-CoV-2. For this reason, to be able to delineate the widespread coverage of antiviral activities of MXenes, viral genotypes carrying the wild type (clade “other”) and mutated spike (clades GR, GH and S) have been included in this study.

For evaluating MXene antiviral activity towards SARS-COV-2, we first selected $Ti_3C_2T_x$, the most widely used MXene type for biomedical applications. *In vitro* viral infection against SARS-CoV-2 was performed in the presence of the material in Vero E6 cells by using the four selected different viral clades. Vero E6 cells are widely used in viral studies in literature due to their suitability for propagating replicative viruses [68,69]. In order to quantify viral copy number, culture supernatants after viral infection were analyzed via qRT-PCR. As shown in Fig. 3A, when cells were infected with SARS-CoV-2 in the presence of $Ti_3C_2T_x$, the viral copy number of GR clade was significantly reduced at every dilution tested, as compared to the cells treated with the virus alone; more than 99% inhibition was achieved already at 1:3,125 dilution. On the other hand, for the other genotypes, no significant effect was observed (Fig. 3B–D). This finding critically suggests the importance of considering the viral genotypes and mutations while testing antiviral activity of nanomaterials and any other candidate molecule. Indeed, the presence of D614G mutation on spike, which has been found to be in GR and GH genotypes in our study (Fig. 2C), has been shown to increase viral infection by creating structural changes at the receptor binding domains of viral particles to ACE2 receptors [66–69]. To further corroborate the inhibition phenomenon observed in GR clade, we assessed the viability of Vero E6 cells following infection. The viability of Vero E6 cells was significantly improved in the presence of the material, as compared to the cells treated with the virus alone (Fig. 3E). Also, no toxicity was observed when the cells were treated with only the nanomaterial (Fig. 3F); $Ti_3C_2T_x$ showed antiviral activity starting from 1:3,125 dilution. IC50 concentration was equal to 0.32 µg/mL, which is effective considering the usual doses (below 100 µg/mL) used in the biomedical field [22,28,29]. Based on these findings, we selected viral particles from the clade GR to test other MXenes: $Ta_4C_3T_x$, $Mo_2Ti_2C_3T_x$ and $Nb_4C_3T_x$. As shown in Fig. 2, $Ta_4C_3T_x$ and $Nb_4C_3T_x$ did not show any significant change in viral copy number (Fig. 4A and C) whereas $Mo_2Ti_2C_3T_x$ was able to induce more than 95% of viral inhibition at 100 µg/mL (Fig. 4B). Titanium oxide (TiO_2) nanoparticles were used as a nanoparticle control group (Fig. 4D) in order to show that MXene dependent viral inhibition was not only due to the presence of titanium in the structure. Finally, in order to further examine the effect of non-Ti MXenes on other clades of SARS-CoV-2, we have performed the antiviral activity assessment of the $Ta_4C_3T_x$ and $Nb_4C_3T_x$ on the clades S and “other”. The genotypes from these two clades have mutations specifically different than the D614G one which have been already tested in the clades GR and GH. Results showed that similar to the response obtained with the clade GR, there is no antiviral activity obtained with these materials (Fig. 4E and F).

We then selected $Ti_3C_2T_x$, the most potent of the tested materials against SARS-CoV-2 particles, as a model to investigate the mechanisms underlying its antiviral activity. To this end, we carried out *in silico* molecular docking analysis to study the MXene targeted proteins and pathways during viral pathogenesis. The interactions of $Ti_3C_2T_x$ with different SARS-CoV-2 protein domains that have been shown to be the most important for SARS-CoV-2 infection were investigated[70] (Fig. 5A, B). The binding energies involved during these interactions were not found to be high or show any viral protein domain-dependent variation (Fig. 5A). When the types of bondings were analyzed, although various weak interactions have been detected including metal, pi-alkyl, alkyl or van der Waals, hydrogen bonding was not observed (Fig. 5B and Fig. S1).

The binding energies of $Ti_3C_2T_x$ with viral proteins were found to be similar to each other, suggesting that there could be other effective targets or important pathways in the viral infection cycle. Therefore, a proteomic analysis was performed to better explain the mechanism behind the viral inhibition. We performed LC-MS/MS analysis of Vero E6 cells following material exposure. The proteome analyses revealed a total of 158 differentially expressed proteins. Among them, upon material treatment, 90 proteins were up-regulated and 68 down-regulated ($p < 0.05$). The proteins were classified by gene ontology (GO) annotation according to molecular function, biological process and cellular compartment. The analysis contains several cellular compartment (CC) ontology terms and shows a high proportion of proteins associated with extracellular exosome which is known to be associated with membrane trafficking (Fig. 5C). Many proteins were also assigned to GO Biological Process (BP) and Molecular Function (MF) terms and the results demonstrated a high prevalence of proteins with nucleosome assembly and poly(A) RNA binding activity, respectively (Figs. S2A and B). The KEGG pathways with the most significant change in material treatment are associated with metabolic pathways, viral carcinogenesis and RNA

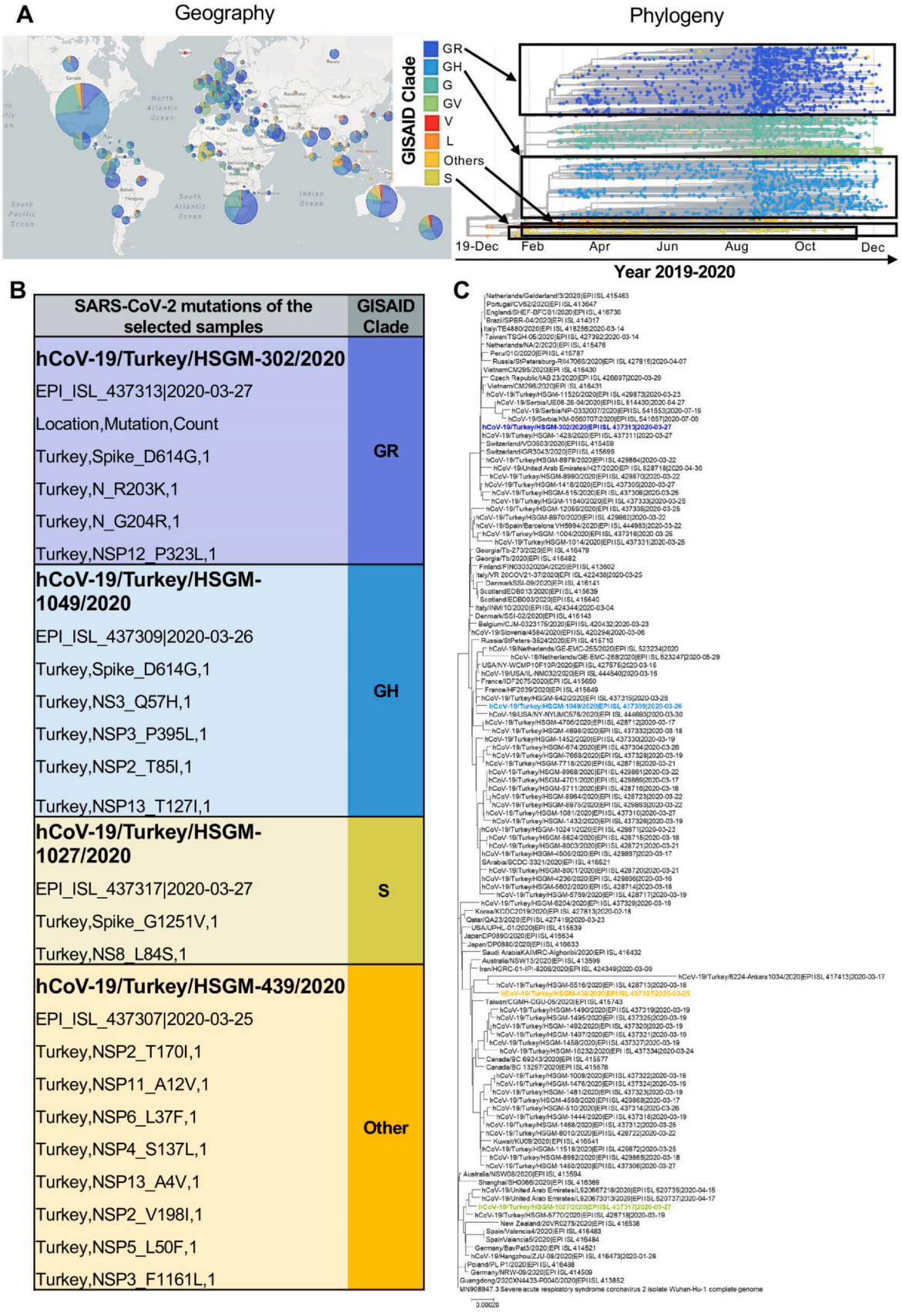

SARS-CoV-2 mutations of the selected samples	GISAID Clade
hCoV-19/Turkey/HSGM-302/2020	
EPI_ISL_437313|2020-03-27	
Location,Mutation,Count	
Turkey,Spike_D614G,1	GR
Turkey,N_R203K,1	
Turkey,N_G204R,1	
Turkey,NSP12_P323L,1	
hCoV-19/Turkey/HSGM-1049/2020	
EPI_ISL_437309|2020-03-26	
Turkey,Spike_D614G,1	
Turkey,NS3_Q57H,1	GH
Turkey,NSP3_P395L,1	
Turkey,NSP2_T85I,1	
Turkey,NSP13_T127I,1	
hCoV-19/Turkey/HSGM-1027/2020	
EPI_ISL_437317|2020-03-27	S
Turkey,Spike_G1251V,1	
Turkey,NS8_L84S,1	
hCoV-19/Turkey/HSGM-439/2020	
EPI_ISL_437307|2020-03-25	
Turkey,NSP2_T170I,1	
Turkey,NSP11_A12V,1	
Turkey,NSP6_L37F,1	Other
Turkey,NSP4_S137L,1	
Turkey,NSP13_A4V,1	
Turkey,NSP2_V198I,1	
Turkey,NSP5_L50F,1	
Turkey,NSP3_F1161L,1	

Fig. 2. SARS-CoV-2 characterization: geographical distribution, phylogeny, genotypes and mutations identification. A) GISAID clades of SARS-CoV-2 are represented according to their geographical distribution and phylogeny. Genomes (3510) sampled by GISAID between Dec 2019 and Dec 2020 are pictured (www.gisaid.org) and selected clades (GR, GH, Others and S) within this study are highlighted in black boxes. B) Details of viral genotypes and mutations used in this study. Four different viral clades of SARS-CoV-2 were used, mutations and GISAID classification of each genotype are provided. C) The phylogenetic tree of the studied viruses in reference to the Wuhan-Hu-1/2019.

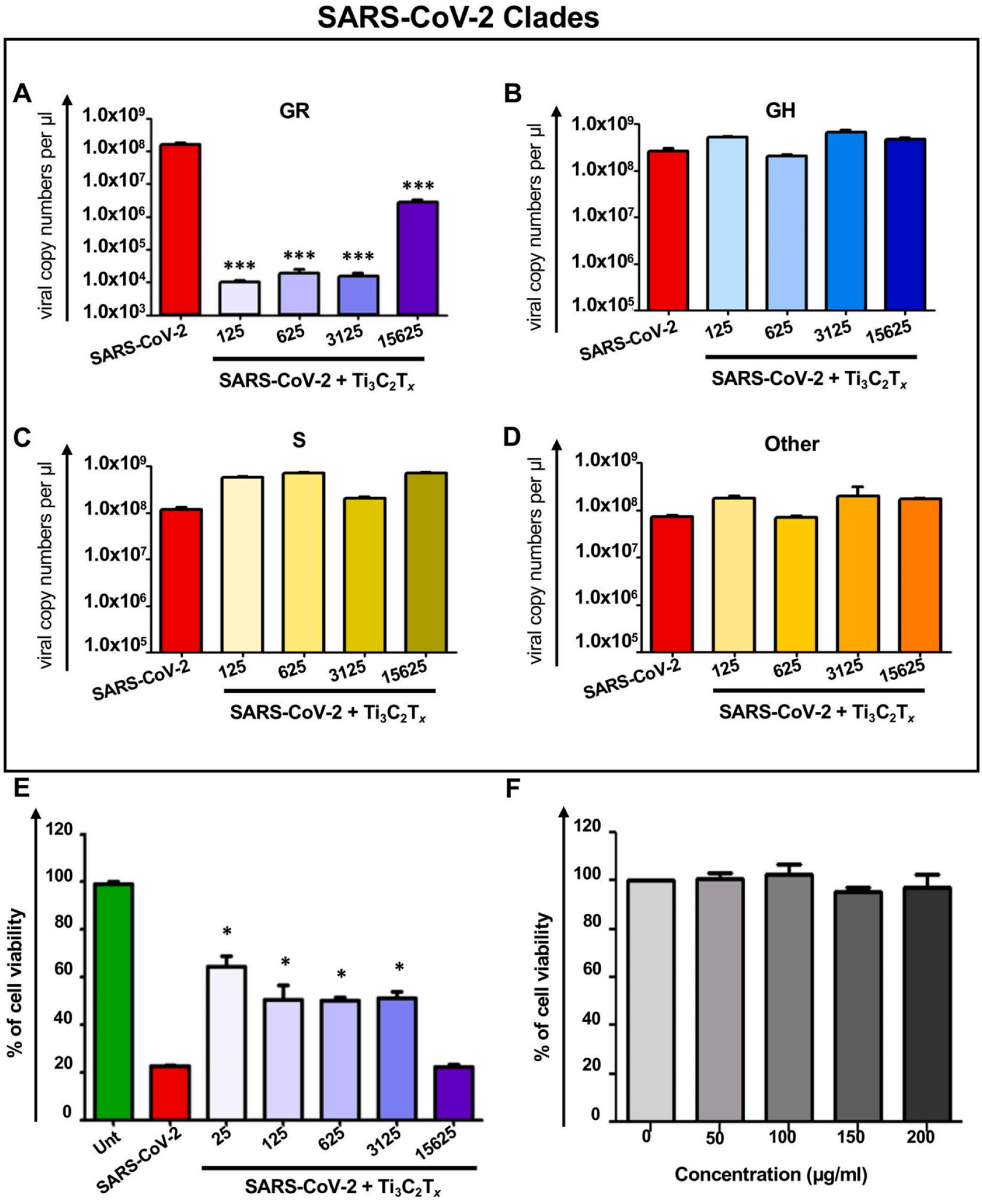

Fig. 3. Antiviral activity of $Ti_3C_2T_x$ on the infection of selected genotypes and mutations of SARS-CoV-2. Vero E6 cells were infected with SARS-CoV-2 in the presence of $Ti_3C_2T_x$ at different dilutions (from a stock concentration of 1.1 mg/mL) and after 48 h, viral copies in cell culture supernatant were analyzed via qRT-PCR. The four different viral genotypes selected and characterized: A) GR, B) GH, C) S and D) other. E) Vero E6 cells were infected with SARS-CoV-2 in the presence of $Ti_3C_2T_x$ at different dilutions (from a stock concentration of 1.1 mg/mL) and after 48 h, viability of cells was assessed and percentage of viability was plotted. F) Toxicity of $Ti_3C_2T_x$ was determined in Vero E6 cells following material exposure for 4 h. Percentage of viability was assessed via LDH assay. Statistical differences: *$p < 0.05$; ***$p < 0.001$ compared to only virus group. Three independent samples were analyzed for each sample group.

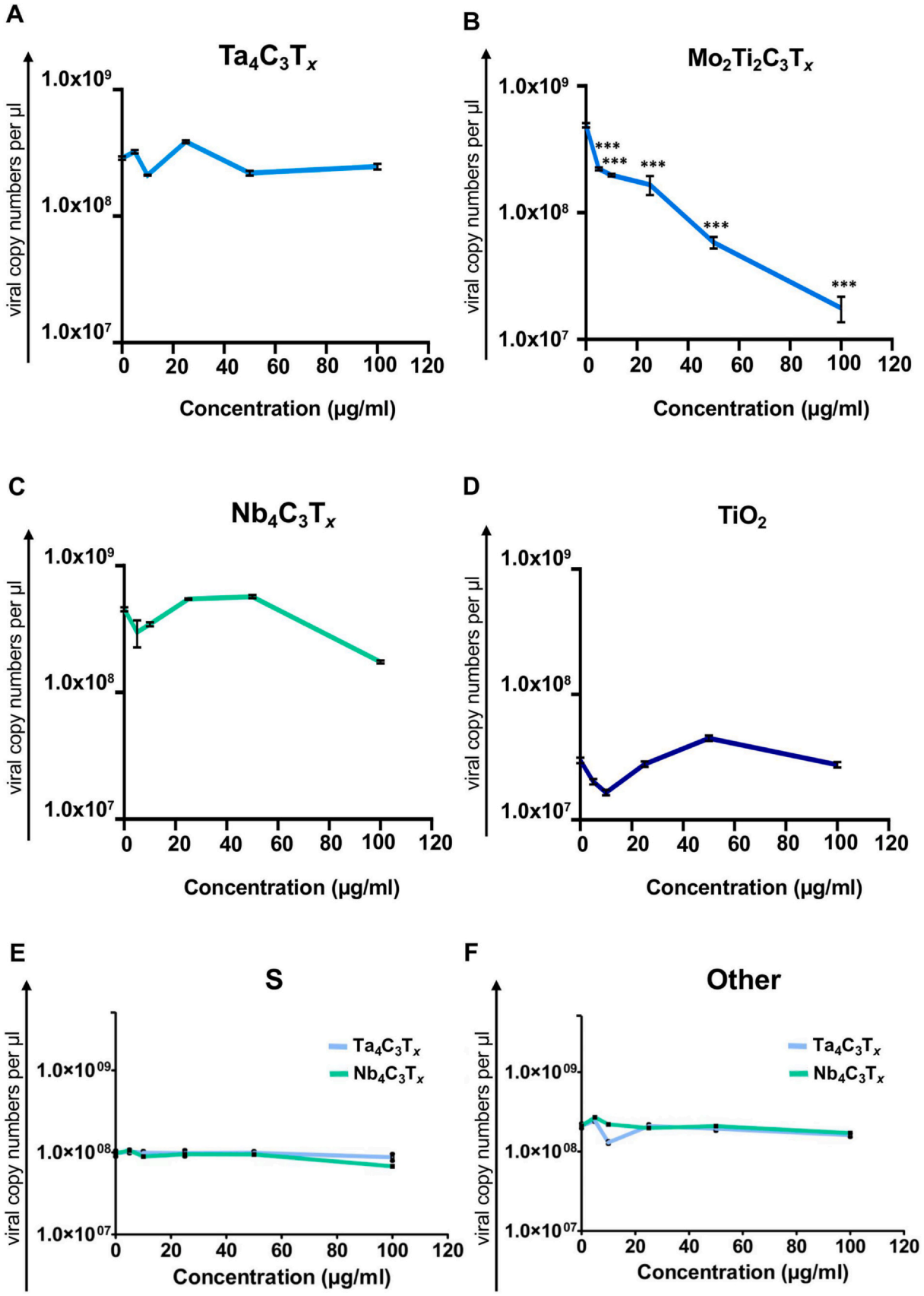

Fig. 4. Antiviral activity of a panel MXenes and TiO_2 nanoparticles on SARS-CoV-2 infection. Vero E6 cells were infected with SARS-CoV-2 (clade GR) in the presence of a panel of Mxenes A) $Ta_4C_3T_x$, B) $Mo_2Ti_2C_3T_x$ and C) $Nb_4C_3T_x$ at different material concentration. Viral copy numbers in cell culture supernatant were analyzed via qRT-PCR. D) TiO_2 nanoparticles were used as a comparative group. Vero E6 cells were infected with SARS-CoV-2 (clade GR) in the presence of TiO_2. Viral copies in cell culture supernatant were analyzed via qRT-PCR. In order to evaluate the activity of non-Ti MXenes ($Ta_4C_3T_x$ and $Nb_4C_3T_x$) in detail, Vero E6 cells were infected with SARS-CoV-2 from **E)** clade S and F) clade "other" in the presence of materials at different concentration. Viral copy numbers in cell culture supernatant were analyzed via qRT-PCR. Statistical differences: $^{*}p < 0.05$; $^{***}p < 0.001$ compared to only virus group. Three independent samples were analyzed for each sample group.

A

	BINDING ENERGY ΔG, (kcal/mol)
6VWW	-3.56
6LU7	-3.10
6M0J	-3.55
6M03	-3.25
6VXX	-3.60
6VYB	-3.64

B

	METAL	PI-ALKYL	ALKYL	VAN DER WAALS
6VWW	3	2	2	1
6LU7	1	0	8	0
6M0J	3	1	1	0
6M03	1	3	3	0
6VXX	3	5	2	0
6VYB	1	0	2	0

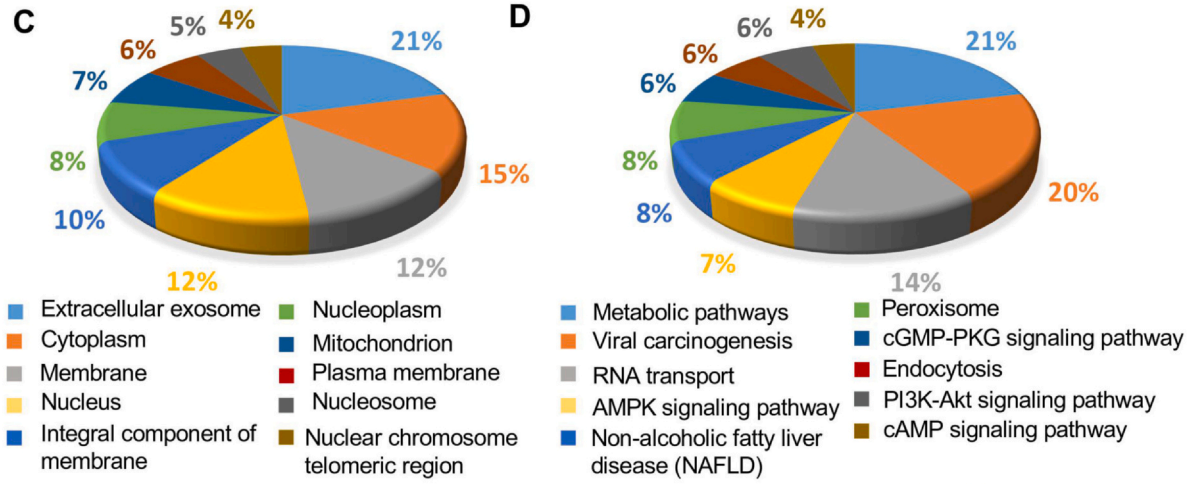

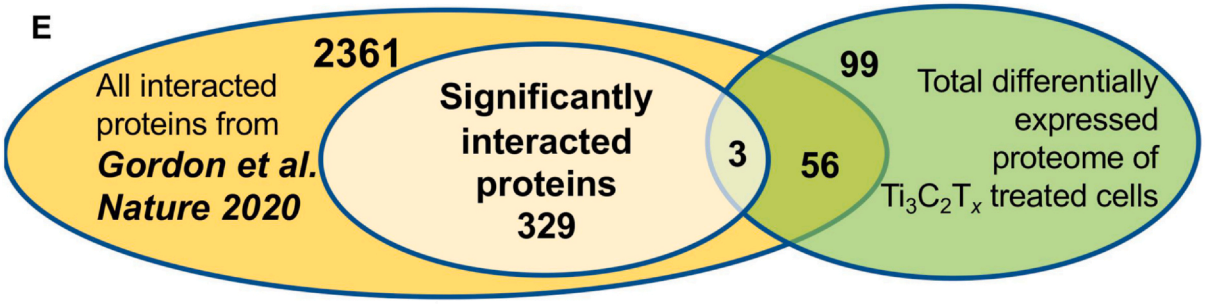

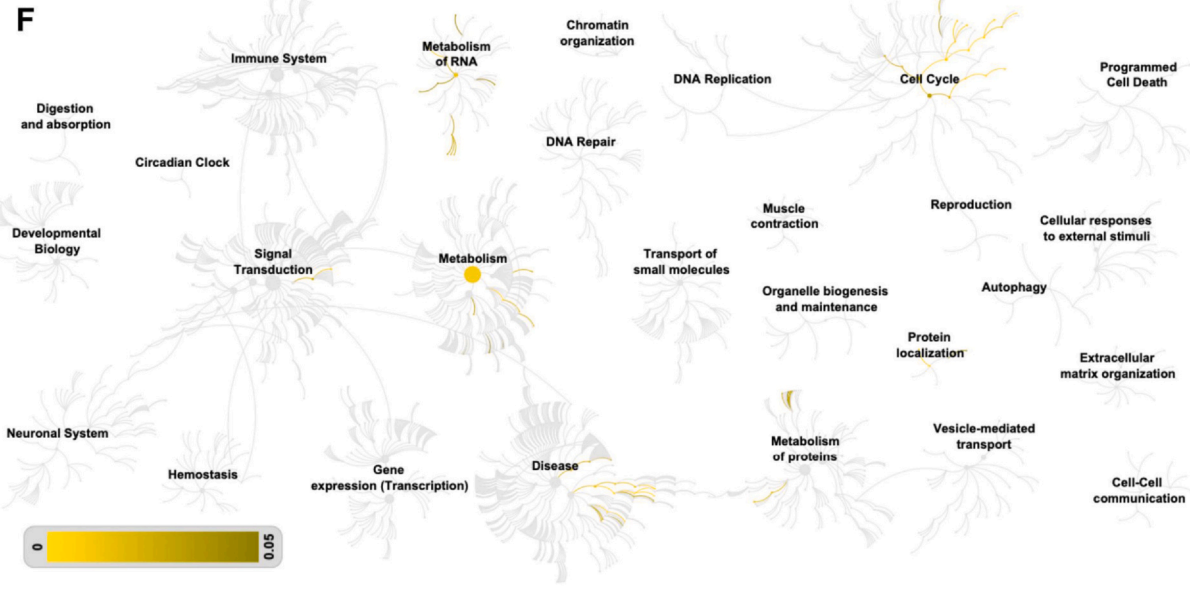

(caption on next page)

Fig. 5. Molecular docking, proteomic analysis and comparison to the SARS-CoV-2 protein interaction map to delineate the antiviral mechanism of MXene. A) *In silico* molecular docking analysis of Ti_3C_2 against different viral protein domains (6VWW, 6LU7, 6M0J, 6M03, 6VXX and 6VYB) was performed and binding energies were identified. B) Interaction types and numbers of these interactions were identified following molecular docking analysis. Vero E6 cells were treated with $Ti_3C_2T_x$ and cellular total proteins were isolated for LC-MS/MS analysis. GO annotation was performed for C) cellular compartment and D) KEGG pathways. E) The SARS-CoV-2 protein interaction map has been published [64], reporting protein interactions between SARS-CoV-2 proteins and human proteins. A Venn diagram was constructed in order to compare $Ti_3C_2T_x$ treated cellular proteome with the SARS-CoV-2 protein interaction map [64]. A total of 59 proteins were overlapping between the two datasets. The significantly interacted proteins were found to be GNG5, GRPEL1 and NUTF2 (3 proteins at the intersection of the Venn diagram). F) Reactome pathway analysis of these 59 overlapping proteins with the SARS-CoV-2 protein interaction map [64] was performed and the whole reactome image is represented. Scale bar represents p value from 0 to 0.05. Three independent samples were analyzed for each sample group.

transport (Fig. 5D). A genome-wide overview of the Reactome pathway analysis identified that cell cycle and DNA repair are the over-represented pathways within the analyzed proteins (Fig S3).

Shortly after the start of the pandemic, the SARS-CoV-2 protein interaction map was published in Nature by Gordon et al. [71]. In this study, 26 of the 29 SARS-CoV-2 proteins were cloned and expressed in human cells which allowed the identification of the human proteins physically associated with each viral protein using affinity-purification mass spectrometry. Authors have reported that among these protein interactions (in total of 2749) between SARS-CoV-2 proteins and human proteins, 332 were high-confidence proteins. A comparison analysis between our dataset and the significantly interacted proteins from the study by Gordon et al. (332 in total) revealed that a total of 59 SARS-CoV-2 interacted proteins are also identified in the $Ti_3C_2T_x$ protein dataset (Table S1). Among them, GNG5, GRPEL1 and NUTF2 are significantly interacted proteins when compared to Gordon et al. [71] (Fig. 5E). The Reactome pathway analysis of these 59 overlapping proteins showed that cell cycle and metabolism of RNA are the most represented pathways for those overlapped proteins (Fig. 5F). The network analysis for the 332 significantly interacted SARS-CoV-2 proteins and 59 overlapped differentially expressed proteins of material response shows numerous connections between the proteins (Fig. S4). The significantly interacted proteins, GNG5, GRPEL1 and NUTF2, were all upregulated compared to the untreated control, based on our proteomic analysis (2.8-, 3- and 2-fold increase, respectively). According to Gordon et al., GNG5, GRPEL1 and NUTF2, interact with viral NSP7, NSP10 and NSP15, respectively. NSP7 have been reported to be important in membrane trafficking and G-protein coupled receptor (GPCR) signaling in SARS-CoV-2 infection. Similarly, NSP15 is involved in vesicle trafficking as well as nuclear transport machinery. Furthermore, NSP7 and NSP10 are among several proteins which can modify endomembrane compartments to favor Coronavirus entry and replication [71]. In addition to this protein interaction map by Gordon et al., other studies have also identified these pathways to be determinant in inhibiting viral infection [72–78]. Taken together, docking analysis, proteomics data, comparison with SARS-CoV-2 protein interaction map provided us the data to depict the mechanism of MXene-dependent antiviral activity (Fig. 6). As described above, $Ti_3C_2T_x$ treatment results in interference with viral life cycle through the interaction with certain SARS-CoV proteins such as NSP7, NSP10 and NSP15. These viral proteins are involved at different pathways and biological processes including membrane trafficking, GPCR signaling, mitochondrial function, metabolic pathways and viral replication. Therefore, MXene has the ability to exert antiviral activity through modulating these viral proteins and pathways important for viral propagation (Fig. 6).

Considering that vaccines now in use for SARS-CoV-2 are based on nanoparticle based drug delivery systems [14–17], and all the multiple potentialities of MXene in nanomdicine, together with the fact that the immune cells functionality play a critical role in every disease including COVID-19, we next evaluated the biocompatibility of $Ti_3C_2T_x$ MXene towards human immune cells. Immortalized human T lymphocytes (Jurkat cells) and human peripheral blood mononuclear cells (PBMCs), purified from healthy donors, were treated with $Ti_3C_2T_x$ for 24 h. After treatment, PBMCs were stained with Fixable Viability Stain 780 to detect necrotic cells, and EtOH 70% was used as positive control. MXene did not induce any significant loss of Jurkat cell (Fig. S5) or PBMC viability as compared to the control (Fig. 7A, Figs. S5D-E and S6A). In addition, $Ti_3C_2T_x$ did not induce any cytotoxic effect also considering CD4 + T cells (Fig. 7B, Fig. S6D) and CD8 + T cells (Fig. 7B, Fig. S6E). The same results were obtained when the cytotoxicity was evaluated in the total number of monocytes (Fig. 7C, Fig. S6F), as well as in classical monocytes (C. monocytes) ($CD14^{high}$ $CD16^{-}$, Fig. 4D, Fig. S6G), intermediate monocytes (Int. monocytes) ($CD14^{high}$ $CD16^{+}$, Fig. 4D, Fig. S6H), and in non-classical monocytes (N.C. monocytes) ($CD14^{low}$ CD16 +, Fig. 7D, Fig. S6I). The anti-inflammatory effects of $Ti_3C_2T_x$ were validated also on stimulated PBMCs population. The level of CD25 activation marker significantly decreased for the PBMCs samples treated with $Ti_3C_2T_x$ + LPS when compared to the negative control and positive control LPS (Fig. S7H and I), confirming a potential anti-inflammatory effect of the nanomaterial. Similarly, the TNFα levels, measured in the supernatants of treated PBMCs, significantly decreased also in correspondence with the treatment with $Ti_3C_2T_x$ + LPS with respect to the positive control LPS.

To gain a comprehensive view of $Ti_3C_2T_x$ impact on 17 different immune cell subpopulations, we took advantage of single-cell mass cytometry (CyTOF) technology. CyTOF became a well-established platform for the most powerful high-dimensional single-cell analysis approaches enabling to discern multiple cellular populations while simultaneously revealing many factors of cellular behavior in a single cell manner [79]. PBMCs were treated with $Ti_3C_2T_x$ (50 μg/mL) for 24 h or left untreated, and EtOH 70% was used as positive control. Following a similar strategy previously reported by us [79], PBMCs were initially gated to discriminate 9 immune cell types according to the expression profile of ten clusters of differentiation (CD) markers present on their cell surface; then we further studied the expression of seven more CD markers to dissect all T cells and B cells subpopulations to a total of 17 cell subpopulations finally identified. The single-cell resolution plot was constructed by applying the viSNE computational approach [80], and nine significant CD 45 + immune cell populations were identified. In detail: T helper cells (Th. cells), cytotoxic T cells (Ct. T cells), C. monocytes, Int. monocytes, N.C. monocytes, natural killer cells (NKs), B cells, myeloid and plasmacytoid dendritic cells (mDCs and pDCs, respectively) (Fig. 7E).

Cisplatin (Cis) staining, that takes advantage of the ability of cisplatin to enter into both late apoptotic and necrotic cells [81], was performed to assess cell viability of PBMC populations at the single-cell level (Fig. 7F) and represented as heat map (Fig. 7G). Notably, the detailed analyses allowed by CyTOF confirmed the total absence of cytotoxicity induced by $Ti_3C_2T_x$ (Fig. S6B and C). Taken together, these findings demonstrate the total absence of $Ti_3C_2T_x$ cytotoxicity for a broad range of distinct immune cell subpopulations.

We next investigated the impact of $Ti_3C_2T_x$ on PBMC functionality by monitoring different activation parameters. $Ti_3C_2T_x$ did not induce any significant change in either CD25 or CD69 expression in total PBMCs (Fig. 8A, B and S7A). Thus, we investigated more in-depth the effect of $Ti_3C_2T_x$ on immune cells by gating T cell subpopulations using CD3, CD4 and CD8 as markers. In line with the results obtained in total PBMCs, no significant change in the expression of CD25 and CD69 was observed in CD4 T cells (Fig. 8C, S7B) and CD8 T cells (Fig. 8D, S7C). Interestingly, $Ti_3C_2T_x$ induced a significant decrease of CD69 expression in total monocytes tracked down specifically to Intermediate Monocytes, leaving CD25 expression unchanged (Fig. 8E-H, S7D-G). These data suggest that MXenes

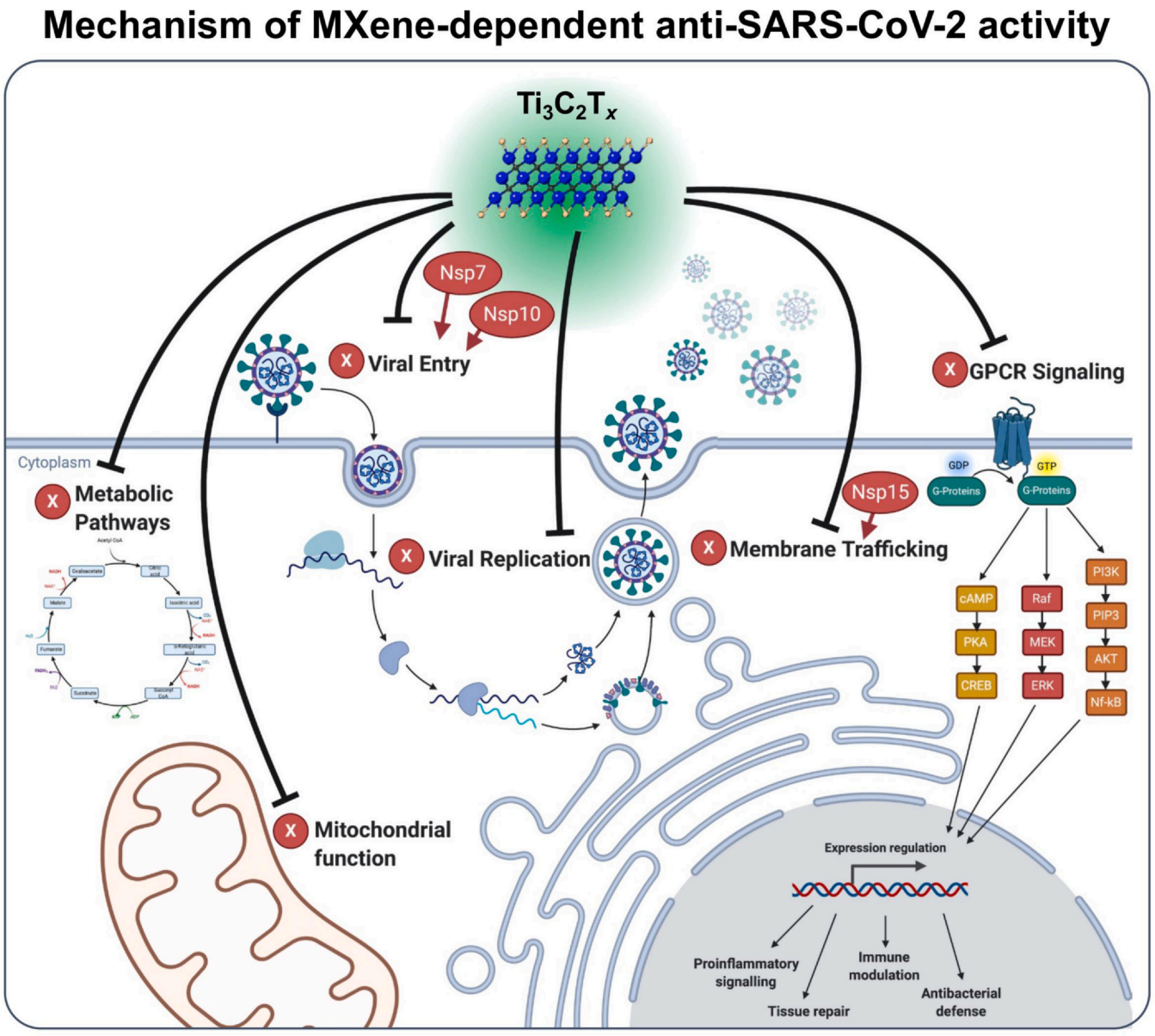

Fig. 6. The mechanism of MXene-dependent viral inhibition. $Ti_3C_2T_x$ exerts its viral inhibition activity not only at the cell surface but also through different signaling mechanisms including membrane trafficking, GPCR signaling, mitochondrial function, metabolic pathways and viral replication. Our results suggest that host proteins such as GNG5, GRPEL1 and NUTF2 have been shown to be important regulators in $Ti_3C_2T_x$ dependent antiviral activity. These host proteins interact with viral NSP7, NSP10 and NSP15 proteins (colored in red), respectively. NSP7 have been reported to be important in membrane trafficking and G-protein coupled receptor (GPCR) signaling in SARS-CoV-2 infection. NSP15 is involved in vesicle trafficking as well as nuclear transport machinery. NSP7 and NSP10 are among several proteins which can modify endomembrane compartments to favor viral entry and replication. Overall, treatment with $Ti_3C_2T_x$ acts on all these pathways in Vero E6 cells leading to the inhibition of SARS-CoV-2 infection.

may reduce Intermediate Monocytes pro-inflammatory activity. We might speculate that MXenes can affect the TLRs stimulation pathway in intermediate monocytes dampening their activation processes. To deepen into the effect elicited by $Ti_3C_2T_x$ on the immune subpopulations, we measured the expression of the activation marker HLA-DR. Interestingly, PBMCs displayed a slight but significant downregulation of HLA-DR that was traced to a reduction observed only in CD4 T cells (Fig. S8). Classical monocytes show a slight increase in HLA-DR expression (Fig. S8). HLA-DR is an MHC class II cell surface molecule that is constitutively expressed, among others, by monocytes to present antigens to T cells. Our data might suggest increased activity in the APC function of monocytes that however, does not elicit a further proinflammatory T cell response but rather regulatory.

One of the main features of COVID-19, especially in the severe form of the disease, is the triggering of a cytokine storm in the body [4,82], resulting in increased circulating levels of IL-6 and TNF-α [83]. Of note, few nanomaterials have been applied to modulate the immune response [84], and carbon-based materials have been shown to be effective in reducing many cytokines in blood, including IL-6 and TNF-α [85]. Thus, to further investigate the functional impact of $Ti_3C_2T_x$ on the immune cell subpopulations, we applied CyTOF to monitor the production of five different cytokines (i.e., IL-6, TNF-α, IL-17a, IL-17f, IFN-γ) at the single-cell level. In addition, two different proteins that mark the activation status of immune cells, i.e., Perforin and Granzyme B (GrB), were evaluated. The heat map displayed the median expression values of all the cytokines in respect to each immune subpopulation (Fig. 9A and Fig. S9). $Ti_3C_2T_x$ did not induce any change in IL-6 production (Fig. S9A) due to its early release. Instead, TNF-α levels were significantly decreased in all the immune subpopulations, with the only exception of activated CT cells, pDCs, and B cell subsets (Fig. S9B). These results, together with the neutral

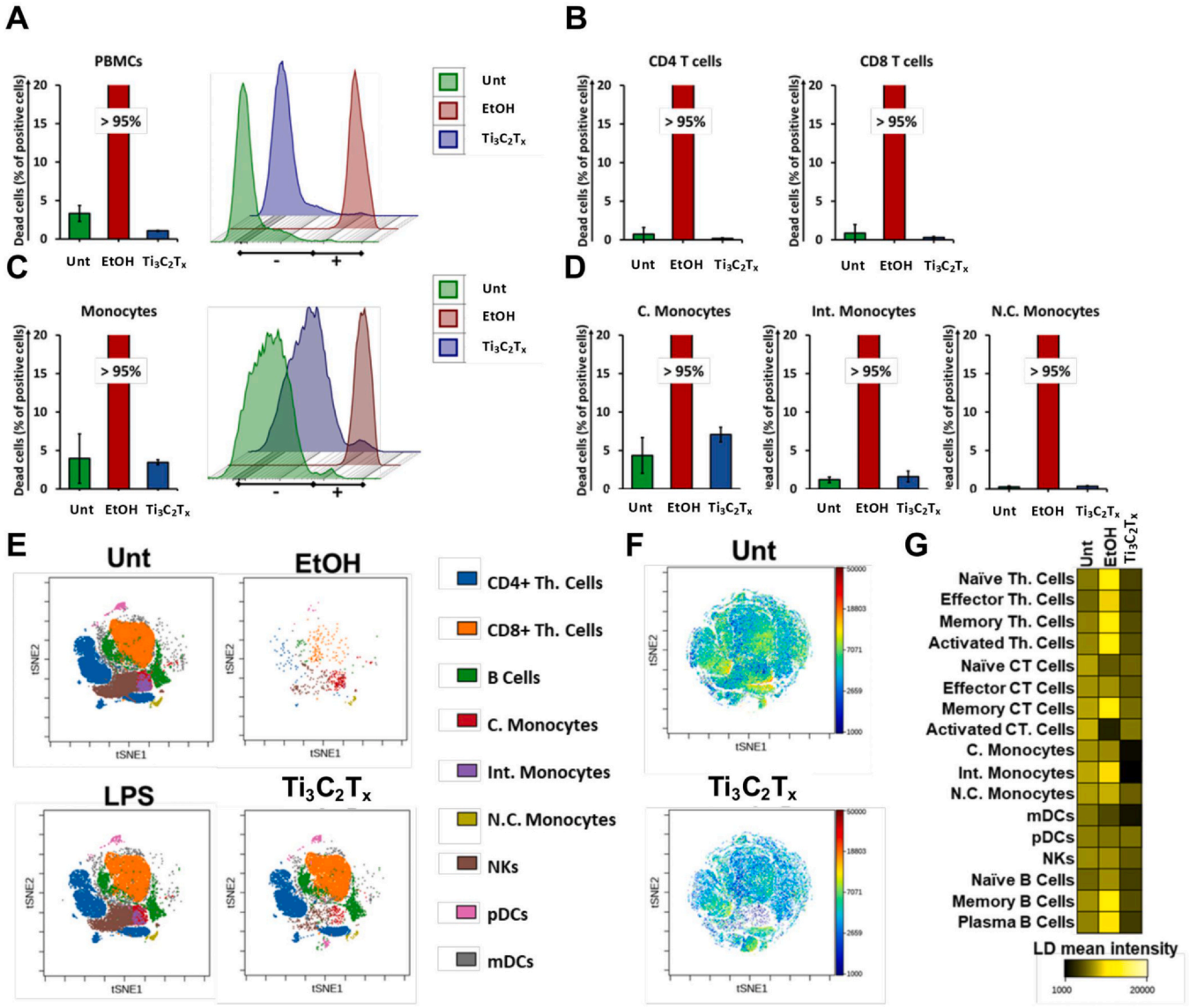

Fig. 7. Viability on peripheral blood mononuclear cell pool and on the distinct immune cell subpopulations at the single-cell level. Cell viability staining analysis by flow cytometry CyTOF. PBMCs were treated with $Ti_3C_2T_x$ (50 μg/mL) for 24 h or left untreated (Unt). EtOH 70% was used as a positive control to induce cell death. A) PBMCs were stained with Fixable Viability Staining 780. Necrotic cells were evaluated and expressed as percentage of total cell number. Data are presented as bar graph (left panel) and histogram plot (right panel). B) Cell death in CD4 T cells (left panel) and in CD8 T cells (right panel) expressed as percentage of total cell number. C) Monocytes were stained with Fixable Viability Staining 780. Necrotic cells were evaluated and expressed as percentage of total cell number. Data are presented as bar graph (left panel) and histogram plot (right panel). D) Cell death in C. monocytes (left panel), Int. monocytes (mid panel), and N.C. monocytes (right panel) expressed as percentage of total cell number. E) The viSNE analysis clusterization report the single-cell subpopulation identified out of PBMCs. Uncalled cells are not showed. Immune cells cluster morphology after treatment with $Ti_3C_2T_x$ are reported. F) viSNE single cell analyst showing the LD mean marker expression ratio for untreated and $Ti_3C_2T_x$ -treated immune cells. G) Heat map of LD mean marker expression ratio for all gated immune subpopulations. Three independent samples were analyzed for each sample group.

effect of $Ti_3C_2T_x$ on CD25 and CD69 expression in CD4 T cells (Fig. S7B), and the concomitant decrease of HLA-DR expression (Fig. S8A), recognized as a marker of inflammation of T cells [86], suggest that $Ti_3C_2T_x$ skewed T cells toward an anti-inflammatory phenotype. The reduction of TNF-α levels in all monocyte subpopulations (Fig. S9B) and the reduction of IFN-γ levels in C. monocytes further support the anti-inflammatory effect of $Ti_3C_2T_x$ (Fig. S9C). Moreover, $Ti_3C_2T_x$ induced the downregulation of Perforin (Fig. S9D) and GrB (Fig. S9E), proteins that synergize to mediate apoptosis of target cells upon pro-inflammatory stimuli [87,88], in a large number of cell subsets, while no changes were observed in IL17-a and IL17-f levels (Fig. S9F-G).

To further investigate the impact of MXene on immune cells, a comprehensive panel of 40 cytokines and chemokines was examined by Luminex technology using the BioRad Bio-Plex Pro human Chemokine panel 40 plex (cat#171AK99MR2). PBMCs supernatants were collected after treatment with $Ti_3C_2T_x$ (24 h). The panel includes the key mediators involved in the pathophysiology of COVID-19 cytokine storm: TNF-α, IL-1β, IL-2, GM-CSF, CCL2, IFN-γ, and IL-6 [89,90]. It also includes other cytokines often dysregulated in many immunologic disorders and infectious diseases, including SARS-CoV-2 infection (Fig. 9B). The fold regulation values for 24 h treatment are displayed as heat map (Fig. 9B). The data for each cytokine and summary statistics are reported in Table S2. As compared to the untreated control, $Ti_3C_2T_x$ caused a downregulation of the production of central inflammation-related mediators, overall inducing an inhibitory effect. In particular, $Ti_3C_2T_x$ significantly inhibited the production of the chemokine CCL24, an eosinophil chemotactic protein. A similar, strong, downregulation was exerted on the production of other mediators consistent with an inhibition of the

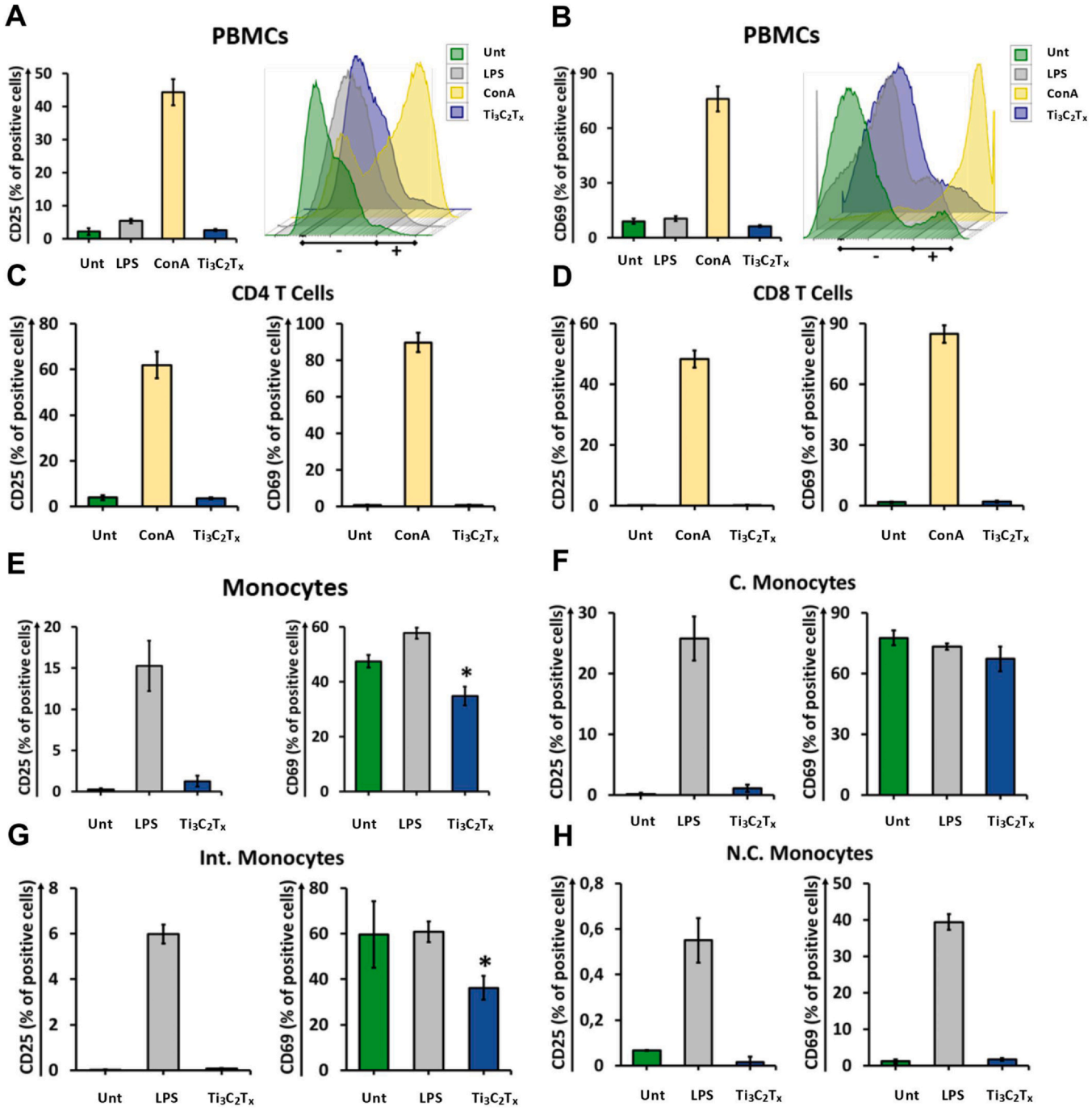

Fig. 8. Analysis of activation on peripheral blood mononuclear cells and monocytes. Cell activation staining analysis by flow cytometry. Cells were treated with 50 μg/mL $Ti_3C_2T_x$ for 24 h or left untreated (Unt). LPS (2 μg/mL) was used as a positive control for PBMCs while ConA (10 μg/mL) was used as positive control for T cells. A) PBMCs were stained with CD25-PE. Cell activation was evaluated and expressed as percentage of total cell number. Data are presented as bar graph (left panel) and histogram plot (right panel). B) PBMCs were stained with CD69-PE-Cy7. Cell activation was evaluated and expressed as percentage of total cell number. Data are presented as bar graph (left panel) and histogram plot (right panel). C) CD4 T cells were stained with CD25-PE (left panel) and CD69-PE-Cy7 (right panel), and cell activation was evaluated and expressed as percentage of total cell number. D) CD8 T cells were stained with CD25-PE (left panel) and CD69-PE-Cy7 (right panel), and cell activation was evaluated and expressed as percentage of total cell number. E) Monocytes were stained with CD25-PE (left panel) and CD69-PE-Cy7 (right panel). Cell activation was evaluated and expressed as percentage of total cell number. F) C. monocytes were stained with CD25-PE (left panel) and CD69-PE-Cy7 (right panel), and cell activation was evaluated and expressed as percentage of total cell number. G) Int. monocytes were stained with CD25-PE (left panel) and CD69-PE-Cy7 (right panel), and cell activation was evaluated and expressed as percentage of total cell number. H) N.C. monocytes were stained with CD25-PE (left panel) and CD69-PE-Cy7 (right panel), and cell activation was evaluated and expressed as percentage of total cell number. Data are presented as mean ± ST.D. of three independent samples. *P < 0.05 by one-way ANOVA Tukey's multiple comparison test.

innate-adaptive immune response crosstalk, such as CXCL9, CXCL10 and CXCL11, which are classic IFN-γ, stimulated chemokines, and of IFN-γ itself [91,92]. CXCL9–11 are critical for the recruitment of monocytes and activated T and NK cells in the lung through CXCR3 binding [93,94]. Specifically, CXCL10 is a key mediator of SARS-CoV-2 acute respiratory distress syndrome (ARDS) [93–97] and has been identified as a strong biomarker COVID-19 disease severity and as an independent predictor of disease progression [93,97]. Targeting CXCL10-CXCR3 pathway have been hypothesized in this setting [93] and anti-IFN-γ monoclonal antibodies and JAK1/2 inhibitors, which

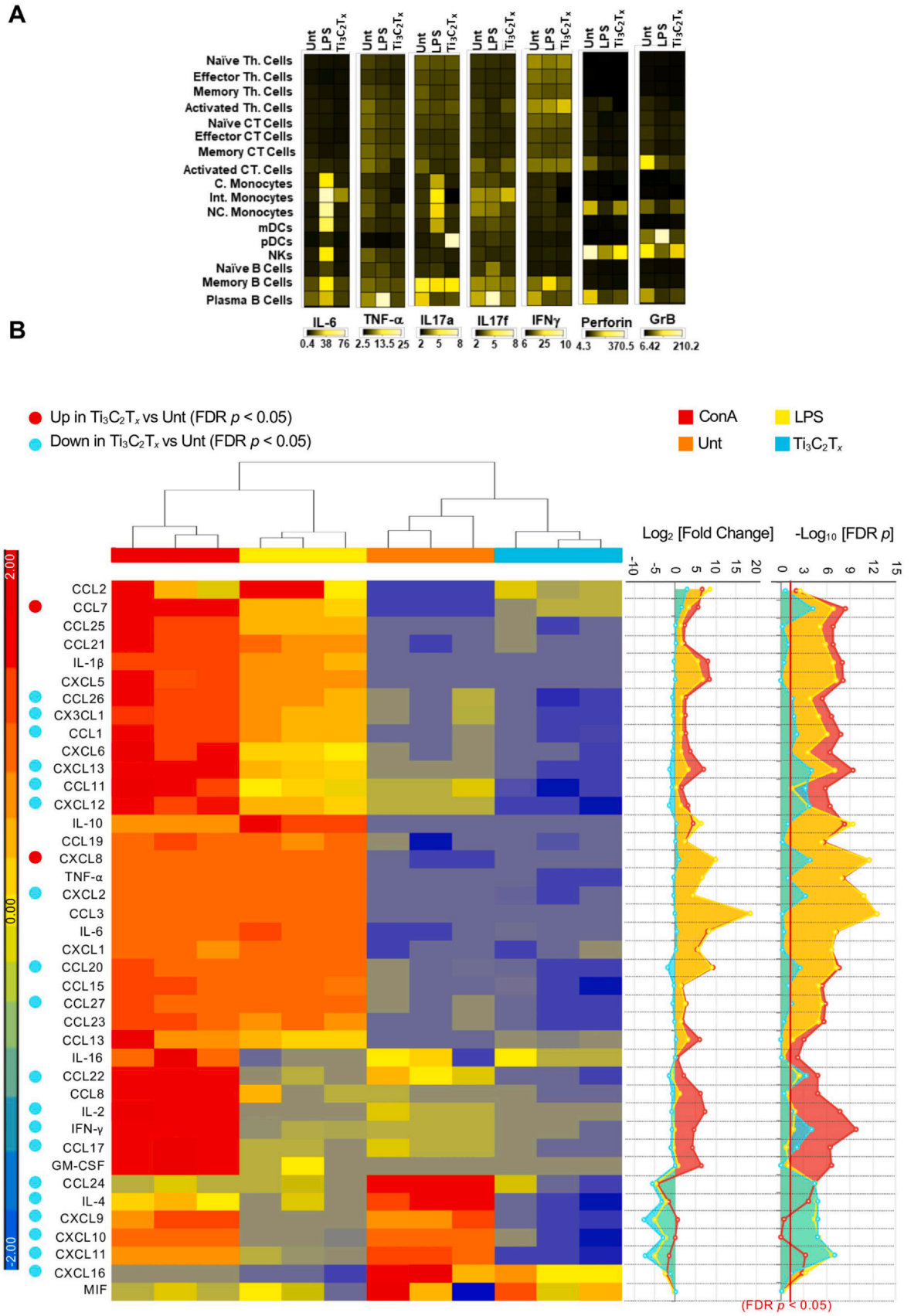

(caption on next page)

Fig. 9. Functionality of peripheral blood mononuclear cell pool and on the distinct immune cell subpopulations at the single-cell level. Cell functionality analysis by CyTOF and Luminex technology. PBMCs were treated with $Ti_3C_2T_x$ (50 μg/mL) for 24 h or left untreated (Unt). EtOH 70% was used as a positive control to induce cell death. A) Bar graph of cisplatin (LD) mean marker expression ratio for all T cell, monocyte, DC, NK, and B cell subpopulations. Heatmaps were generated on the concatenated files. Data are presented as mean ± ST.D. of three independent samples. B) Hierarchical clustering of inflammatory mediators released by PBMCs treated with 50 μg/mL of $Ti_3C_2T_x$ for 24 h. As positive control, cells were exposed to ConA (10 μg/mL) and LPS (2 μg/mL). Heatmaps (left panel) represents the z-score of the Log_2 concentration for each cytokine. The right panels display the Log_2 Fold Change of each experimental conditions as compared to negative controls (Unt) and the corresponding negative Log_{10} *p* values corrected for multiple tests (Benjamini and Hochberg false discovery rate, FDR), computed using ANOVA contrasts. The red bar represents the *p* value cut-off (FDR < 0.05); z-score range for color coding was set between + 2 and − 2 (blue = down-regulated cytokines, negative z-score; red = up-regulated cytokines, positive z-score). Three independent samples were analyzed for each sample group.

blocks IFN-γ signaling, are currently in phase 3 clinical trial testing for the treatment of SARS-CoV ARDS [89] (NCT0432402, AND NCT04358614 respectively). In addition, $Ti_3C_2T_x$ significantly inhibited the production of IL-2 and IL-4, which have been also involved in COVID-19 disease severity [98], and their inhibition through JAK1/JAK3 blockade is currently being tested in phase 2 clinical trials (NCT04332042). Moreover, the immune inhibitory effect induced by $Ti_3C_2T_x$ was accompanied by a neutral effect on other cytokine-storm key mediators (IL-6, TNF-α, IL-1β, and CCL2), and by a significant suppression of other inflammatory chemokines such as CXCL2, CXCL12, CXCL13, CXCL16, CX3CL1, CCL1, CCL11, CCL17, CCL20, CCL20, CCL26–27, and CCL22. The only two proteins significantly upregulated by $Ti_3C_2T_x$ were the chemokines CCL7 and CXCL8, which have not been reported as main mediators of the cytokine-release syndrome [89,90]. Although elevated levels of CCL7 have been recently observed in one COVID-19 study [97], this was observed in concert with the release of other cytokines and it was probably related to a downstream activation following hyperinflammation. As such, it is unlikely to represent, in isolation, a causal agent of COVID-19 severity.

Discussion

2D materials have been suggested to be novel effective bactericidal agents due to their physicochemical properties. These materials have been shown to interact with microorganisms both physically and chemically. Furthermore, due to their outstanding photothermal and photocatalytic properties, 2D materials can effectively help to eradicate even typically drug-resistant microorganisms [25,99]. Antimicrobial resistance (AMR) has been referred to be the most significant threat to the global health and economy in recent years, and now the scene is taken over by COVID-19 [1]. Therefore, it is of great importance to understand and evaluate how 2D materials can help our fight against viral threats. Nanomaterials have been used in different ways against viral infections. First, due to their antimicrobial properties, nanomaterials can provide alternative methods to classical disinfection protocols used in healthcare settings [5]. By leveraging their affinity towards viral particles, nanomaterials can be used to entrap viral particles and improve infiltration rates on face masks [4,6,7]. As a recent example, De Maio et al. reported that graphene nanoplatelets- and GO-based integration into face masks and other PPE enhances their protection efficacy significantly increasing their protection against the SARS-CoV-2 virus [8]. Finally, these materials have been shown to be effective antiviral drug delivery systems for various viral-based pathologies [100,101].

MXenes are a fast-growing family of 2D materials with diverse chemistries and structures. The use of MXenes in biomedical fields is recently emerging with pioneering examples in the photothermal therapy of cancer, theranostics, biosensors, dialysis, and neural electrodes [31,39,44–47,102–104]. $Ti_3C_2T_x$, in particular, a member of this family, has shown promising antibacterial activities in various studies, as previously demonstrated [48,49,54,105]. Therefore, we hypothesized that $Ti_3C_2T_x$ can show antiviral activity. To test this hypothesis, in this study, we first performed viral infection in vitro with SARS-CoV-2 of different viral clades as classified by GISAID, in the presence of different types of MXenes. Our results suggested that $Ti_3C_2T_x$ and $Mo_2Ti_2C_3T_x$ demonstrate antiviral activity even at low concentrations. The fact that TiO_2 nanoparticles did not inhibit viral infection in our study further supports that it is not the presence of titanium that gives MXenes an antiviral property. Polar, negatively charged, and redox active surfaces of MXenes can strongly interact with viral proteins leading to viral inhibition. The fact that two MXenes with the same structure but different layers of surface atoms show antiviral activity suggests that the surface chemistry is the key parameter. This allows us to search for other antiviral MXenes among Ti- and Mo-based compositions, such as Ti_2CT_x, Mo_2CT_x, $Mo_{4/3}CT_x$ $Mo_2Ti_2C_2T_x$, and their solid solutions. In addition to material characteristics, our results showed that the genotypes and mutations are important determinant of antiviral activity. Both the GR and GH clades have a mutation at the spike, which is the D614G mutation. The GR clade showed more sensitivity against the MXenes compared to the GH clade, pointing out the importance of mutations also in other viral proteins including non-structural genes. For example, the GH clade has mutations on the non-structural genes which have not been studied enough in the current literature in terms of their effect on viral infectivity. On the other hand, the S clade has a different spike mutation known as G1251V, which is not within the receptor binding domain of the viral spike, and therefore it is not expected to play an important role in spike-receptor binding and complex formation. The clade represented as "other" didn't show any mutation on the viral spike, representing a native form of the spike protein. In summary, our data suggested that the viral genotypes and mutations that will be emerging in the near future should be considered carefully in future studies.

Until now, various nanoparticles have been shown to inhibit SARS-CoV-2 infection in vitro [106–109]. However, there is limited or no data available for their mechanism of action on the viral particles. Understanding the mechanism of inhibition is an important step in the development nanomaterials to be used against COVID-19. For this reason, we performed detailed *in silico* and proteomic analyses to better understand how these materials interact with viral proteins and whether they can interfere with viral infection cycle. The binding energies of $Ti_3C_2T_x$ with viral proteins was found to be quite similar to each other suggesting that additional in-depth molecular analysis is needed to better understand the mechanism behind. Considering that *in silico* analyses were performed with viral protein domains which have been shown to be important for viral infection in literature [70], our findings suggest that there could be other effective targets or important pathways in the viral infection cycle. Therefore, a proteomic analysis was performed to further investigate the fundamental mechanism behind viral inhibition from $Ti_3C_2T_x$. Via functional annotation studies based on proteomic data, we demonstrated that $Ti_3C_2T_x$ can interfere with viral life cycle via different mechanisms including membrane trafficking, GPCR signaling and mitochondrial function. This result suggests that $Ti_3C_2T_x$ exerts its viral inhibition activity not only at the cell surface but also through different signaling mechanisms important in viral life cycle. These results also contribute towards our understanding of molecular mechanisms involved in COVID-19 and provide insights on some of the relevant pathways and proteins that should be targeted when developing antiviral drug or nanomaterial.

The concept of nanoimmunity-by-design [23] can help scientists to design 2D materials for immune modulation, either by stimulating or suppressing the immune reaction and it would find specific applications in the context of vaccine development for SARS-CoV-2 or to counteract the cytokine storm induced by COVID-19, respectively [4]. For example,

with the help of long-studied lipid based nanosystems, mRNA-based vaccines are expected to save millions of lives. The efficacy and safety of these nano delivery platforms have been reported extensively in literature [110–113] and is of a paramount importance when evaluating candidate nanomaterials for antiviral applications. Therefore, in order to better show the applicability and suitability of MXenes in antiviral research, we conducted a thorough analysis of the immunomodulation activity of $Ti_3C_2T_x$. Our results show that $Ti_3C_2T_x$ is not cytotoxic in any PBMC population, which supports the high biocompatibility of this material. Following this characterization, we further evaluated the immune profile of $Ti_3C_2T_x$. According to our data, this material does not activate PBMCs and reduce pro-inflammatory cytokines. These results suggest an anti-inflammatory effect elicited by $Ti_3C_2T_x$. Nevertheless, further studies are necessary to elucidate whether the reduced level of different cytokines observed in Th cells and monocytes (e.g., TNF-α) could be due to a direct effect of $Ti_3C_2T_x$ on cells or to a removal of inflammatory cytokines as shown using other carbon-based nanomaterials [85,114].

Conclusion

In conclusion, our study demonstrates the antiviral activity of MXenes against SARS-CoV-2. In addition, we established the high bio and immune compatibility of MXenes as well as their anti-inflammatory effects on human immune cells. Our results serve as a guide to direct future studies to implement MXenes and other 2D nanomaterials in different biomedical technologies and nanomedicine tools, particularly against viral diseases, as well as any immune-system related syndromes.

CRediT authorship contribution statement

Mehmet Altay Unal: Conceptualization, Methodology, Analysis, Writing. **Fatma Bayrakdar:** Conceptualization, Methodology, Analysis, Writing. **Laura Fusco:** Conceptualization, Methodology, Analysis, Writing, Visualization. **Omur Besbinar:** Analysis, Visualization, Writing. **Christopher E. Shuck:** Conceptualization, Methodology, Writing. **Süleyman Yalcin:** Methodology, Analysis. **Mine Turktas Erken:** Methodology, Analysis, Data curation. **Aykut Ozkul:** Conceptualization, Methodology. **Cansu Gurcan:** Analysis, Writing, Visualization. **Oguzhan Panatli:** Analysis. **Gokce Yagmur Summak:** Methodology, Data curation. **Cemile Gokce:** Analysis. **Marco Orecchioni:** Methodology, Analysis, Writing. **Arianna Gazzi:** Methodology, Analysis, Visualization. **Flavia Vitale:** Conceptualization, Writing. **Julia Somers:** Analysis, Data curation. **Emek Demir:** Conceptualization, Data curation. **Serap Suzuk Yildiz:** Methodology, Analysis. **Hasan Nazir:** Methodology, Analysis. **Jean-Charles Grivel:** Methodology, Analysis, Writing. **Davide Bedognetti:** Methodology, Analysis, Writing. **Andrea Crisanti:** Conceptualization, Writing. **Kamil Can Akcali:** Conceptualization, Writing. **Yury Gogotsi:** Conceptualization, Analysis, Writing, Project administration. **Lucia Gemma Delogu:** Conceptualization, Analysis, Visualization, Writing, Project administration. **Açelya Yilmazer:** Conceptualization, Analysis, Visualization, Writing, Project administration.

Declaration of Competing Interest

The authors declare that they have no known competing financial interests or personal relationships that could have appeared to influence the work reported in this paper.

Acknowledgement

MAU, AO, HN, KCA and AY would like to acknowledge the funding from the Scientific and Technological Research Council of Turkey (TUBITAK) under the grant number 18AG020. AY is thankful to the Turkish Academy of Sciences (TUBA) for financial support under the young investigator programme. L.G.D., D.B., and L.F. would like to acknowledge the financial support from the European Union's Horizon 2020 research and innovation programme under the Marie Sklodowska-Curie grant agreement no. 734381 (CARBO-IMmap) and Sidra Precision Medicine Program (SDR400025). LGD acknowledges the Starting Grant 2020 from the Department of Biomedical Science, University of Padua. Synthesis of MXenes for biomedical applications at Drexel University was supported by the U.S. National Science Foundation under grant no. 2035007. The schematic representation of MXene dependent viral inhibition in Fig. 6 was created with BioRender.com.

Appendix A. Supporting information

Supplementary data associated with this article can be found in the online version at doi:10.1016/j.nantod.2021.101136.

References

[1] A.K. Murray, The novel coronavirus COVID-19 outbreak: global implications for antimicrobial resistance, Front. Microbiol. 11 (2020) 1020.
[2] E. Dong, H. Du, L. Gardner, An interactive web-based dashboard to track COVID-19 in real time, Lancet Infect. Dis 20 (2020) 533–534.
[3] M.A. Knobler, S.L. Mahmoud A, The Threat of Pandemic Influenza: Are We Ready? Workshop Summary, National Academies Press (US), Washington (DC), 2005.
[4] C. Weiss, M. Carriere, L. Fusco, I. Capua, J.A. Regla-Nava, M. Pasquali, J.A. Scott, F. Vitale, M.A. Unal, C. Mattevi, D. Bedognetti, A. Merkoçi, E. Tasciotti, A. Yilmazer, Y. Gogotsi, F. Stellacci, L.G. Delogu, Toward nanotechnology-enabled approaches against the COVID-19 pandemic, ACS Nano 14 (2020) 6383–6406.
[5] S. Talebian, G.G. Wallace, A. Schroeder, F. Stellacci, J. Conde, Nanotechnology-based disinfectants and sensors for SARS-CoV-2, Nat. Nanotechnol. 15 (2020) 618–621.
[6] E.V.R. Campos, A.E.S. Pereira, J.L. de Oliveira, L.B. Carvalho, M. Guilger-Casagrande, R. de Lima, L.F. Fraceto, How can nanotechnology help to combat COVID-19? Opportunities and urgent need, J. Nanobiotechnol. 18 (2020) 125.
[7] P.K. Rai, Z. Usmani, V.K. Thakur, V.K. Gupta, Y.K. Mishra, Tackling COVID-19 pandemic through nanocoatings: confront and exactitude, Curr. Opin. Green Sustain. Chem. 3 (2020) 100011-100011.
[8] F. De Maio, V. Palmieri, G. Babini, A. Augello, I. Palucci, G. Perini, A. Salustri, M. De Spirito, M. Sanguinetti, G. Delogu, L.G. Rizzi, G. Cesareo, P. Soon-Shiong, M. Sali, M. Papi, Graphene nanoplatelet and graphene oxide functionalization of face mask materials inhibits infectivity of trapped SARS-CoV-2 (2020) (medRxiv) 2020.2009.2016.20194316.
[9] M. Abbas, M. Ovais, C. Chen, Phage capsid nanoparticles as multivalent inhibitors of viral infections, Sci. Bull. 65 (2020) 2050–2052.
[10] P.A.S. Kinaret, G. Del Giudice, D. Greco, COVID-19 acute responses and possible long term consequences: what nanotoxicology can teach us, Nano Today 35 (2020) 100945100945-100945.
[11] V. Palmieri, M. Papi, Can graphene take part in the fight against COVID-19? Nano Today 33 (2020) 100883.
[12] I.R.S. Ribeiro, R.F. da Silva, C.P. Silveira, F.E. Galdino, M.B. Cardoso, Nano-targeting lessons from the SARS-CoV-2, Nano Today 36 (2021) 101012.
[13] L. He, J. Zhao, L. Wang, Q. Liu, Y. Fan, B. Li, Y.-L. Yu, C. Chen, Y.-F. Li, Using nano-selenium to combat coronavirus disease 2019 (COVID-19)? Nano Today 36 (2021) 101037101037-101037.
[14] Z. Tang, N. Kong, X. Zhang, Y. Liu, P. Hu, S. Mou, P. Liljeström, J. Shi, W. Tan, J.S. Kim, Y. Cao, R. Langer, K.W. Leong, O.C. Farokhzad, W. Tao, A materials-science perspective on tackling COVID-19, Nat. Rev. Mater. 5 (2020) 847–860.
[15] Z. Zhang, Z. Tang, N. Farokhzad, T. Chen, W. Tao, Sensitive, rapid, low-cost, and multiplexed COVID-19 monitoring by the wireless telemedicine platform, Matter. 3 (2020) 1818–1820.
[16] W. Tao, N. Kong, X. Ji, Y. Zhang, A. Sharma, J. Ouyang, B. Qi, J. Wang, N. Xie, C. Kang, H. Zhang, O.C. Farokhzad, J.S. Kim, Emerging two-dimensional monoelemental materials (Xenes) for biomedical applications, Chem. Soc. Rev. 48 (2019) 2891–2912.
[17] C. Liu, J. Shin, S. Son, Y. Choe, N. Farokhzad, Z. Tang, Y. Xiao, N. Kong, T. Xie, J.S. Kim, W. Tao, Pnictogens in medicinal chemistry: evolution from erstwhile drugs to emerging layered photonic nanomedicine, Chem. Soc. Rev. (2021).
[18] Z. Tang, X. Zhang, Y. Shu, M. Guo, H. Zhang, W. Tao, Insights from nanotechnology in COVID-19 treatment, Nano Today 36 (2021) 101019.
[19] M.D. Shin, S. Shukla, Y.H. Chung, V. Beiss, S.K. Chan, O.A. Ortega-Rivera, D.M. Wirth, A. Chen, M. Sack, J.K. Pokorski, N.F. Steinmetz, COVID-19 vaccine development and a potential nanomaterial path forward, Nat. Nanotechnol. 15 (2020) 646–655.
[20] Y.H. Chung, V. Beiss, S.N. Fiering, N.F. Steinmetz, COVID-19 vaccine frontrunners and their nanotechnology design, ACS Nano 14 (2020) 12522–12537.

[21] Nanomedicine and the COVID-19 vaccines, Nat. Nanotechnol., 15, 2020, 963–963.

[22] L. Fusco, A. Gazzi, G. Peng, Y. Shin, S. Vranic, D. Bedognetti, F. Vitale, A. Yilmazer, X. Feng, B. Fadeel, C. Casiraghi, L.G. Delogu, Graphene and other 2D materials: a multidisciplinary analysis to uncover the hidden potential as cancer theranostics, Theranostics 10 (2020) 5435–5488.

[23] A. Gazzi, L. Fusco, M. Orecchioni, S. Ferrari, G. Franzoni, J.S. Yan, M. Rieckher, G. Peng, M.A. Lucherelli, I.A. Vacchi, N.D.Q. Chau, A. Criado, A. Istif, D. Mancino, A. Dominguez, H. Eckert, E. Vázquez, T.D. Ros, P. Nicolussi, V. Palermo, B. Schumacher, G. Cuniberti, Y. Mai, C. Clementi, M. Pasquali, X. Feng, K. Kostarelos, A. Yilmazer, D. Bedognetti, B. Fadeel, M. Prato, A. Bianco, L.G. Delogu, Graphene, other carbon nanomaterials and the immune system: toward nanoimmunity-by-design, J. Phys. Mater. 3 (2020) 034009.

[24] B. Pelaz, C. Alexiou, R.A. Alvarez-Puebla, F. Alves, A.M. Andrews, S. Ashraf, L.P. Balogh, L. Ballerini, A. Bestetti, C. Brendel, S. Bosi, M. Carril, W.C. Chan, C. Chen, X. Chen, X. Chen, Z. Cheng, D. Cui, J. Du, C. Dullin, A. Escudero, N. Feliu, M. Gao, M. George, Y. Gogotsi, A. Grünweller, Z. Gu, N.J. Halas, N. Hampp, R.K. Hartmann, M.C. Hersam, P. Hunziker, J. Jian, X. Jiang, P. Jungebluth, P. Kadhiresan, K. Kataoka, A. Khademhosseini, J. Kopeček, N.A. Kotov, H.F. Krug, D.S. Lee, C.M. Lehr, K.W. Leong, X.J. Liang, M. Ling Lim, L.M. Liz-Marzán, X. Ma, P. Macchiarini, H. Meng, H. Möhwald, P. Mulvaney, A.E. Nel, S. Nie, P. Nordlander, T. Okano, J. Oliveira, T.H. Park, R.M. Penner, M. Prato, V. Puntes, V.M. Rotello, A. Samarakoon, R.E. Schaak, Y. Shen, S. Sjöqvist, A.G. Skirtach, M.G. Soliman, M.M. Stevens, H.W. Sung, B.Z. Tang, R. Tietze, B.N. Udugama, J.S. VanEpps, T. Weil, P.S. Weiss, I. Willner, Y. Wu, L. Yang, Z. Yue, Q. Zhang, Q. Zhang, X.E. Zhang, Y. Zhao, X. Zhou, W.J. Parak, Diverse applications of nanomedicine, ACS Nano 11 (2017) 2313–2381.

[25] W. Sun, F.-G. Wu, Two-dimensional materials for antimicrobial applications: graphene materials and beyond, Chem. Asian 13 (2018) 3378–3410.

[26] C. Martín, K. Kostarelos, M. Prato, A. Bianco, Biocompatibility and biodegradability of 2D materials: graphene and beyond, Chem. Comm. 55 (2019) 5540–5546.

[27] R. Kurapati, K. Kostarelos, M. Prato, A. Bianco, Biomedical uses for 2D materials beyond graphene: current advances and challenges ahead, Adv. Mater. 28 (2016) 6052–6074.

[28] H. Taheri, M.A. Unal, M. Sevim, C. Gurcan, O. Ekim, A. Ceylan, Z. Syrgiannis, K.C. Christoforidis, S. Bosi, O. Ozgenç, M.J. Gómez, M. Turktas Erken, Ç. Soydal, Z. Eroğlu, C.V. Bitirim, U. Cagin, F. Arı, A. Ozen, O. Kuçuk, L.G. Delogu, M. Prato, Ö. Metin, A. Yilmazer, Photocatalytically active graphitic carbon nitride as an effective and safe 2D material for in vitro and in vivo photodynamic therapy, Small 16 (2020) 1904619.

[29] A. Gazzi, L. Fusco, A. Khan, D. Bedognetti, B. Zavan, F. Vitale, A. Yilmazer, L.G. Delogu, Photodynamic therapy based on graphene and MXene in cancer theranostics, Front. Bioeng. Biotechnol. 7 (2019) 295-295.

[30] M. Naguib, M. Kurtoglu, V. Presser, J. Lu, J. Niu, M. Heon, L. Hultman, Y. Gogotsi, M.W. Barsoum, Two-dimensional nanocrystals produced by exfoliation of Ti_3AlC_2, Adv. Mater. 23 (2011) 4248–4253.

[31] Y. Gogotsi, B. Anasori, The rise of MXenes, ACS Nano 13 (2019) 8491–8494.

[32] B. Anasori, Y. Xie, M. Beidaghi, J. Lu, B.C. Hosler, L. Hultman, P.R.C. Kent, Y. Gogotsi, M.W. Barsoum, Two-dimensional, ordered, double transition metals carbides (MXenes), ACS Nano 9 (2015) 9507–9516.

[33] G. Deysher, C.E. Shuck, K. Hantanasirisakul, N.C. Frey, A.C. Foucher, K. Maleski, A. Sarycheva, V.B. Shenoy, E.A. Stach, B. Anasori, Y. Gogotsi, Synthesis of Mo_4VAlC_4 MAX phase and two-dimensional Mo_4VC_4 MXene with five atomic layers of transition metals, ACS Nano 14 (2020) 204–217.

[34] M. Han, K. Maleski, C.E. Shuck, Y. Yang, J.T. Glazar, A.C. Foucher, K. Hantanasirisakul, A. Sarycheva, N.C. Frey, S.J. May, V.B. Shenoy, E.A. Stach, Y. Gogotsi, Tailoring electronic and optical properties of mxenes through forming solid solutions, J. Am. Chem. Soc. 142 (2020) 19110–19118.

[35] M. Alhabeb, K. Maleski, B. Anasori, P. Lelyukh, L. Clark, S. Sin, Y. Gogotsi, Guidelines for synthesis and processing of two-dimensional titanium carbide ($Ti_3C_2T_x$ MXene), Chem. Mater. 29 (2017) 7633–7644.

[36] L. Verger, V. Natu, M. Carey, M.W. Barsoum, MXenes: an introduction of their synthesis, select properties, and applications, Trends Chem. 1 (2019) 656–669.

[37] K. Maleski, C.E. Shuck, A.T. Fafarman, Y. Gogotsi, The broad chromatic range of two-dimensional transition metal carbides, Adv. Opt. Mater. 9 (2020) 2001563.

[38] H. Miao, Z. Teng, C. Wang, H. Chong, G. Wang, Recent progress in two-dimensional antimicrobial nanomaterials, Chemistry 25 (2019) 929–944.

[39] K. Huang, Z. Li, J. Lin, G. Han, P. Huang, Two-dimensional transition metal carbides and nitrides (MXenes) for biomedical applications, Chem. Soc. Rev. 47 (2018) 5109–5124.

[40] J. Zheng, J.C. Li, L.H. Zhang, X.J. Chen, Y.D. Yu, H. Huang, Post-graphene 2D materials-based antimicrobial agents: Focus on fabrication strategies and biosafety assessments, J. Mater. Sci. 55 (2020) 7226–7246.

[41] H. Ji, H. Sun, X. Qu, Antibacterial applications of graphene-based nanomaterials: recent achievements and challenges, Adv. Drug Deliv. Rev. 105 (2016) 176–189.

[42] H.E. Karahan, C. Wiraja, C. Xu, J. Wei, Y. Wang, L. Wang, F. Liu, Y. Chen, Graphene materials in antimicrobial nanomedicine: current status and future perspectives, Adv. Healthc. Mater. 7 (2018) 1701406.

[43] L. Shi, J. Chen, L. Teng, L. Wang, G. Zhu, S. Liu, Z. Luo, X. Shi, Y. Wang, L. Ren, The antibacterial applications of graphene and its derivatives, Small 12 (2016) 4165–4184.

[44] C. Dai, Y. Chen, X. Jing, L. Xiang, D. Yang, H. Lin, Z. Liu, X. Han, R. Wu, Two-dimensional tantalum carbide (MXenes) composite nanosheets for multiple imaging-guided photothermal tumor ablation, ACS Nano 11 (2017) 12696–12712.

[45] G.K. Nasrallah, M. Al-Asmakh, K. Rasool, K.A. Mahmoud, Ecotoxicological assessment of $Ti_3C_2T_x$ (MXene) using a zebrafish embryo model, Environ. Sci. Nano 5 (2018) 1002–1011.

[46] X. Ren, M. Huo, M. Wang, H. Lin, X. Zhang, J. Yin, Y. Chen, H. Chen, Highly catalytic niobium carbide (MXene) promotes hematopoietic recovery after radiation by free radical scavenging, ACS Nano 13 (2019) 6438–6454.

[47] W. Feng, R. Wang, Y. Zhou, L. Ding, X. Gao, B. Zhou, P. Hu, Y. Chen, Ultrathin molybdenum carbide MXene with fast biodegradability for highly efficient theory-oriented photonic tumor hyperthermia, Adv. Funct. Mater. 29 (2019) 1901942.

[48] K. Rasool, M. Helal, A. Ali, C.E. Ren, Y. Gogotsi, K.A. Mahmoud, Antibacterial activity of $Ti_3C_2T_x$ MXene, ACS Nano 10 (2016) 3674–3684.

[49] K. Rasool, K.A. Mahmoud, D.J. Johnson, M. Helal, G.R. Berdiyorov, Y. Gogotsi, Efficient antibacterial membrane based on two-dimensional $Ti_3C_2T_x$ (MXene) nanosheets, Sci. Rep. 7 (2017) 1598.

[50] R.P. Pandey, K. Rasool, V.E. Madhavan, B. Aïssa, Y. Gogotsi, K. Mahmoud, Ultrahigh-flux and fouling-resistant membranes based on layered silver/mxene ($Ti_3C_2T_x$) nanosheets, J. Mater. Chem. A 6 (2018) 3522–3533.

[51] A.M. Jastrzębska, E. Karwowska, T. Wojciechowski, W. Ziemkowska, A. Rozmysłowska, L. Chlubny, A. Olszyna, The atomic structure of Ti_2C and Ti_3C_2 MXenes is responsible for their antibacterial activity toward E. coli bacteria, J. Mater. Eng. Perform. 28 (2019) 1272–1277.

[52] Z. Wang, W. Zhu, Y. Qiu, X. Yi, A. von dem Bussche, A. Kane, H. Gao, K. Koski, R. Hurt, Biological and environmental interactions of emerging two-dimensional nanomaterials, Chem. Soc. Rev. 45 (2016) 1750–1780.

[53] I.S. Donskyi, W. Azab, J.L. Cuellar-Camacho, G. Guday, A. Lippitz, W.E.S. Unger, K. Osterrieder, M. Adeli, R. Haag, Functionalized nanographene sheets with high antiviral activity through synergistic electrostatic and hydrophobic interactions, Nanoscale 11 (2019) 15804–15809.

[54] F. Alimohammadi, M. Sharifian, Gh Attanayake N.H., A.C. Thenuwara, Y. Gogotsi, B. Anasori, D.R. Strongin, Antimicrobial properties of 2D MnO_2 and MoS_2 nanomaterials vertically aligned on graphene materials and Ti_3C_2 MXene, Langmuir 34 (2018) 7192–7200.

[55] M. Sametband, I. Kalt, A. Gedanken, R. Sarid, Herpes simplex virus type-1 attachment inhibition by functionalized graphene oxide, ACS Appl. Mater. Interfaces 6 (2014) 1228–1235.

[56] S. Ye, K. Shao, Z. Li, N. Guo, Y. Zuo, Q. Li, Z. Lu, L. Chen, Q. He, H. Han, Antiviral activity of graphene oxide: How sharp edged structure and charge matter, ACS Appl. Mater. Interfaces 7 (2015) 21571–21579.

[57] A.R. Deokar, A.P. Nagvenkar, I. Kalt, L. Shani, Y. Yeshurun, A. Gedanken, R. Sarid, Graphene-based "hot plate" for the capture and destruction of the herpes simplex virus type 1, Bioconjugate Chem. 28 (2017) 1115–1122.

[58] A.F. Rodrigues, L. Newman, D.A. Jasim, I.A. Vacchi, C. Ménard-Moyon, L.E. Crica, A. Bianco, K. Kostarelos, C. Bussy, Immunological impact of graphene oxide sheets in the abdominal cavity is governed by surface reactivity, Arch. Toxicol. 92 (2018) 3359–3379.

[59] M. Orecchioni, C. Ménard-Moyon, L.G. Delogu, A. Bianco, Graphene and the immune system: challenges and potentiality, Adv. Drug Deliv. Rev. 105 (2016) 163–175.

[60] B. Fadeel, C. Bussy, S. Merino, E. Vázquez, E. Flahaut, F. Mouchet, L. Evariste, L. Gauthier, A.J. Koivisto, U. Vogel, C. Martín, L.G. Delogu, T. Buerki-Thurnherr, P. Wick, D. Beloin-Saint-Pierre, R. Hischier, M. Pelin, F. Candotto Carniel, M. Tretiach, F. Cesca, F. Benfenati, D. Scaini, L. Ballerini, K. Kostarelos, M. Prato, A. Bianco, Safety assessment of graphene-based materials: focus on human health and the environment, ACS Nano 12 (2018) 10582–10620.

[61] A. Serra, I. Letunic, V. Fortino, R.D. Handy, B. Fadeel, R. Tagliaferri, D. Greco, Inside nano: a systems biology framework to contextualize the mechanism-of-action of engineered nanomaterials, Sci. Rep. 9 (2019) 179.

[62] M. Shekhirev, C.E. Shuck, A. Sarycheva, Y. Gogotsi, Characterization of mxenes at every step, from their precursors to single flakes and assembled films, Progress Mater. Sci. (2020) 100757.

[63] J. Halim, K.M. Cook, M. Naguib, P. Eklund, Y. Gogotsi, J. Rosen, M.W. Barsoum, X-ray photoelectron spectroscopy of select multi-layered transition metal carbides (MXenes), Appl. Surf. Sci. 362 (2016) 406–417.

[64] C.E. Shuck, A. Sarycheva, M. Anayee, A. Levitt, Y. Zhu, S. Uzun, V. Balitskiy, V. Zahorodna, O. Gogotsi, Y. Gogotsi, Scalable synthesis of $Ti_3C_2T_x$ MXene, Adv. Eng. Mater. 22 (2020) 1901241.

[65] X. Tang, C. Wu, X. Li, Y. Song, X. Yao, X. Wu, Y. Duan, H. Zhang, Y. Wang, Z. Qian, J. Cui, J. Lu, On the origin and continuing evolution of SARS-CoV-2, Natl. Sci. Rev. 7 (2020) 1012–1023.

[66] S. Isabel, L. Graña-Miraglia, J.M. Gutierrez, C. Bundalovic-Torma, H.E. Groves, M.R. Isabel, A. Eshaghi, S.N. Patel, J.B. Gubbay, T. Poutanen, D.S. Guttman, S.M. Poutanen, Evolutionary and structural analyses of SARS-CoV-2 D614G spike protein mutation now documented worldwide, Sci. Rep. 10 (2020) 14031.

[67] I.O. Omotuyi, O. Nash, O.B. Ajiboye, C.G. Iwegbulam, E.B. Oyinloye, O.A. Oyedeji, Z.A. Kashim, K. Okaiyeto, Atomistic simulation reveals structural mechanisms underlying D614G spike glycoprotein-enhanced fitness in SARS-CoV-2, J. Comput. Chem. 41 (2020) 2158–2161.

[68] Q. Li, J. Wu, J. Nie, L. Zhang, H. Hao, S. Liu, C. Zhao, Q. Zhang, H. Liu, L. Nie, H. Qin, M. Wang, Q. Lu, X. Li, Q. Sun, J. Liu, L. Zhang, X. Li, W. Huang, Y. Wang, The impact of mutations in SARS-CoV-2 spike on viral infectivity and antigenicity, Cell 182 (2020) 1284–1294 e1289.

[69] B. Korber, W.M. Fischer, S. Gnanakaran, H. Yoon, J. Theiler, W. Abfalterer, N. Hengartner, E.E. Giorgi, T. Bhattacharya, B. Foley, K.M. Hastie, M.D. Parker, D.G. Partridge, C.M. Evans, T.M. Freeman, T.I. de Silva, A. Angyal, R.L. Brown, L. Carrilero, L.R. Green, D.C. Groves, K.J. Johnson, A.J. Keeley, B.B. Lindsey,

P.J. Parsons, M. Raza, S. Rowland-Jones, N. Smith, R.M. Tucker, D. Wang, M.D. Wyles, C. McDanal, L.G. Perez, H. Tang, A. Moon-Walker, S.P. Whelan, C.C. LaBranche, E.O. Saphire, D.C. Montefiori, Tracking changes in SARS-CoV-2 spike: evidence that D614G increases infectivity of the COVID-19 virus, Cell 182 (2020) 812–827 e819.

[70] S. Gervasoni, G. Vistoli, C. Talarico, C. Manelfi, A.R. Beccari, G. Studer, G. Tauriello, A.M. Waterhouse, T. Schwede, A. Pedretti, A comprehensive mapping of the druggable cavities within the SARS-CoV-2 therapeutically relevant proteins by combining pocket and docking searches as implemented in pockets 2.0, IJMS 21 (2020) 5152.

[71] D.E. Gordon, G.M. Jang, M. Bouhaddou, J. Xu, K. Obernier, K.M. White, M.J. O'Meara, V.V. Rezelj, J.Z. Guo, D.L. Swaney, T.A. Tummino, R. Hüttenhain, R.M. Kaake, A.L. Richards, B. Tutuncuoglu, H. Foussard, J. Batra, K. Haas, M. Modak, M. Kim, P. Haas, B.J. Polacco, H. Braberg, J.M. Fabius, M. Eckhardt, M. Soucheray, M.J. Bennett, M. Cakir, M.J. McGregor, Q. Li, B. Meyer, F. Roesch, T. Vallet, A. Mac Kain, L. Miorin, E. Moreno, Z.Z.C. Naing, Y. Zhou, S. Peng, Y. Shi, Z. Zhang, W. Shen, I.T. Kirby, J.E. Melnyk, J.S. Chorba, K. Lou, S.A. Dai, I. Barrio-Hernandez, D. Memon, C. Hernandez-Armenta, J. Lyu, C.J.P. Mathy, T. Perica, K.B. Pilla, S.J. Ganesan, D.J. Saltzberg, R. Rakesh, X. Liu, S.B. Rosenthal, L. Calviello, S. Venkataramanan, J. Liboy-Lugo, Y. Lin, X.-P. Huang, Y. Liu, S.A. Wankowicz, M. Bohn, M. Safari, F.S. Ugur, C. Koh, N.S. Savar, Q.D. Tran, D. Shengjuler, S.J. Fletcher, M.C. O'Neal, Y. Cai, J.C.J. Chang, D.J. Broadhurst, S. Klippsten, P.P. Sharp, N.A. Wenzell, D. Kuzuoglu-Ozturk, H.-Y. Wang, R. Trenker, J.M. Young, D.A. Cavero, J. Hiatt, T.L. Roth, U. Rathore, A. Subramanian, J. Noack, M. Hubert, R.M. Stroud, A.D. Frankel, O.S. Rosenberg, K.A. Verba, D.A. Agard, M. Ott, M. Emerman, N. Jura, M. von Zastrow, E. Verdin, A. Ashworth, O. Schwartz, C. d'Enfert, S. Mukherjee, M. Jacobson, H.S. Malik, D.G. Fujimori, T. Ideker, C.S. Craik, S.N. Floor, J.S. Fraser, J.D. Gross, A. Sali, B.L. Roth, D. Ruggero, J. Taunton, T. Kortemme, P. Beltrao, M. Vignuzzi, A. García-Sastre, K.M. Shokat, B.K. Shoichet, N.J. Krogan, A SARS-CoV-2 protein interaction map reveals targets for drug repurposing, Nature 583 (2020) 459–468.

[72] Y. Singh, G. Gupta, S. Satija, K. Pabreja, D.K. Chellappan, K. Dua, COVID-19 transmission through host cell directed network of GPCR, Drug Dev. Res. 81 (2020) 647–649.

[73] C.A. Birch, O. Molinar-Inglis, J. Trejo, Subcellular hot spots of GPCR signaling promote vascular inflammation, Curr. Opin. Endocr. Metab. Res. 16 (2021) 37–42.

[74] L. Ouyang, J. Gong, Mitochondrial-targeted ubiquinone: a potential treatment for COVID-19, Med. Hypotheses 144 (2020) 110161.

[75] M. Kloc, R.M. Ghobrial, J.Z. Kubiak, The role of genetic sex and mitochondria in response to COVID-19 infection, Int. Arch. Allergy Immunol. 181 (2020) 629–634.

[76] P. Prasun, Letter to the editor: COVID-19, mitochondria, and interferon, J. Interferon Cytokine Res. 40 (2020) 466–467.

[77] K.K. Singh, G. Chaubey, J.Y. Chen, P. Suravajhala, Decoding SARS-CoV-2 hijacking of host mitochondria in COVID-19 pathogenesis, Am. J. Physiol. Cell Physiol. 319 (2020) C258–C267 C258-c267.

[78] K. Wu, J. Zou, H.Y. Chang, RNA-GPS predicts SARS-CoV-2 RNA localization to host mitochondria and nucleolus, Cell Syst. 11 (2020) 102–108.

[79] M. Orecchioni, D. Bedognetti, L. Newman, C. Fuoco, F. Spada, W. Hendrickx, F.M. Marincola, F. Sgarrella, A.F. Rodrigues, C. Ménard-Moyon, G. Cesareni, K. Kostarelos, A. Bianco, L.G. Delogu, Single-cell mass cytometry and transcriptome profiling reveal the impact of graphene on human immune cells, Nat. Commun. 8 (2017) 1109.

[80] A.D. Amir el, K.L. Davis, M.D. Tadmor, E.F. Simonds, J.H. Levine, S.C. Bendall, D.K. Shenfeld, S. Krishnaswamy, G.P. Nolan, D. Pe'er, Visne enables visualization of high dimensional single-cell data and reveals phenotypic heterogeneity of leukemia, Nat. Biotechnol. 31 (2013) 545–552.

[81] H.G. Fienberg, E.F. Simonds, W.J. Fantl, G.P. Nolan, B. Bodenmiller, A platinum-based covalent viability reagent for single-cell mass cytometry, Cytometry A 81 (2012) 467–475.

[82] P. Mehta, D.F. McAuley, M. Brown, E. Sanchez, R.S. Tattersall, J.J. Manson, U.K. Hlh, Across speciality collaboration, COVID-19: consider cytokine storm syndromes and immunosuppression, Lancet 395 (2020) 1033–1034.

[83] G. Chen, D. Wu, W. Guo, Y. Cao, D. Huang, H. Wang, T. Wang, X. Zhang, H. Chen, H. Yu, X. Zhang, M. Zhang, S. Wu, J. Song, T. Chen, M. Han, S. Li, X. Luo, J. Zhao, Q. Ning, Clinical and immunological features of severe and moderate coronavirus disease 2019, J. Clin. Invest. 130 (2020) 2620–2629.

[84] H. Al-Lawati, H.M. Aliabadi, B.S. Makhmalzadeh, A. Lavasanifar, Nanomedicine for immunosuppressive therapy: achievements in pre-clinical and clinical research, Expert Opin. Drug Deliv. 15 (2018) 397–418.

[85] V. Presser, S.H. Yeon, C. Vakifahmetoglu, C.A. Howell, S.R. Sandeman, P. Colombo, S. Mikhalovsky, Y. Gogotsi, Hierarchical porous carbide-derived carbons for the removal of cytokines from blood plasma, Adv. Healthc. Mater. 1 (2012) 796–800.

[86] J.F. Viallard, P. Blanco, M. Andre, G. Etienne, F. Liferman, D. Neau, E. Vidal, J.F. Moreau, J.L. Pellegrin, CD8+HLA-DR+ T lymphocytes are increased in common variable immunodeficiency patients with impaired memory b-cell differentiation, Clin. Immunol. 119 (2006) 51–58.

[87] I. Voskoboinik, J.C. Whisstock, J.A. Trapani, Perforin and granzymes: function, dysfunction and human pathology, Nat. Rev. Immunol. 15 (2015) 388–400.

[88] A.C. Wensink, V. Kemp, J. Fermie, M.I. Garcia Laorden, T. van der Poll, C.E. Hack, N. Bovenschen, Granzyme K synergistically potentiates LPS-induced cytokine responses in human monocytes, Proc. Natl. Acad. Sci. U. S. A. 111 (2014) 5974–5979.

[89] L. Tang, Z. Yin, Y. Hu, H. Mei, Controlling cytokine storm is vital in COVID-19, Front. Immunol. 11 (2020) 570993.

[90] J.R. Tisoncik, M.J. Korth, C.P. Simmons, J. Farrar, T.R. Martin, M.G. Katze, Into the eye of the cytokine storm, Microbiol. Mol. Biol. Rev. 76 (2012) 16–32.

[91] Q. Liu, S. Tomei, M.L. Ascierto, V. De Giorgi, D. Bedognetti, C. Dai, L. Uccellini, T. Spivey, Z. Pos, J. Thomas, J. Reinboth, D. Murtas, Q. Zhang, L. Chouchane, G.R. Weiss, C.L. Slingluff Jr., P.P. Lee, S.A. Rosenberg, H. Alter, K. Yao, E. Wang, F.M. Marincola, Melanoma NOS1 expression promotes dysfunctional IFN signaling, J. Clin. Invest. 124 (2014) 2147–2159.

[92] D. Bedognetti, T.L. Spivey, Y. Zhao, L. Uccellini, S. Tomei, M.E. Dudley, M.L. Ascierto, V. De Giorgi, Q. Liu, L.G. Delogu, M. Sommariva, M.R. Sertoli, R. Simon, E. Wang, S.A. Rosenberg, F.M. Marincola, CXCR3/CCR5 pathways in metastatic melanoma patients treated with adoptive therapy and interleukin-2, Br. J. Cancer 109 (2013) 2412–2423.

[93] M. Blot, M. Jacquier, L.-S. Aho Glele, G. Beltramo, M. Nguyen, P. Bonniaud, S. Prin, P. Andreu, B. Bouhemad, J.-B. Bour, C. Binquet, L. Piroth, J.-P. Pais de Barros, D. Masson, J.-P. Quenot, P.-E. Charles, F. Aptel, A. Dargent, M. Georges, M. Labruyère, L. Lagrost, A. Large, S. Monier, J.-B. Roudaut, C. Thomas, g. Pneumochondrie study, CXCL10 could drive longer duration of mechanical ventilation during COVID-19 ards, Crit. Care 24 (2020) 632.

[94] F. Coperchini, L. Chiovato, L. Croce, F. Magri, M. Rotondi, The cytokine storm in COVID-19: an overview of the involvement of the chemokine/chemokine-receptor system, Cytokine Growth Factor Rev. 53 (2020) 25–32.

[95] Y. Xiong, Y. Liu, L. Cao, D. Wang, M. Guo, A. Jiang, D. Guo, W. Hu, J. Yang, Z. Tang, H. Wu, Y. Lin, M. Zhang, Q. Zhang, M. Shi, Y. Liu, Y. Zhou, K. Lan, Y. Chen, Transcriptomic characteristics of bronchoalveolar lavage fluid and peripheral blood mononuclear cells in COVID-19 patients, Emerg. Microbes Infect. 9 (2020) 761–770.

[96] Y. Yang, C. Shen, J. Li, J. Yuan, M. Yang, F. Wang, G. Li, Y. Li, L. Xing, L. Peng, J. Wei, M. Cao, H. Zheng, W. Wu, R. Zou, D. Li, Z. Xu, H. Wang, M. Zhang, Z. Zhang, L. Liu, Y. Liu, Exuberant Elevation of IP-10, MCP-3 and IL-1 Raduring SARS-CoV-2 Infection is Associated with Disease Severity and Fataloutcome, medRxiv, 2020, 2020.2003.2002.20029975.

[97] Y. Yang, C. Shen, J. Li, J. Yuan, J. Wei, F. Huang, F. Wang, G. Li, Y. Li, L. Xing, L. Peng, M. Yang, M. Cao, H. Zheng, W. Wu, R. Zou, D. Li, Z. Xu, H. Wang, M. Zhang, Z. Zhang, G.F. Gao, C. Jiang, L. Liu, Y. Liu, Plasma IP-10 and MCP-3 levels are highly associated with disease severity and predict the progression of COVID-19, J. Allergy Clin. Immunol. 146 (2020) 119–127 e114.

[98] V.J. Costela-Ruiz, R. Illescas-Montes, J.M. Puerta-Puerta, C. Ruiz, L. Melguizo-Rodríguez, SARS-CoV-2 infection: the role of cytokines in COVID-19 disease, Cytokine Growth Factor Rev. 54 (2020) 62–75.

[99] J. Zheng, J. Li, L. Zhang, X. Chen, Y. Yu, H. Huang, Post-graphene 2D materials-based antimicrobial agents: focus on fabrication strategies and biosafety assessments, J. Mater. Sci. 55 (2020) 7226–7246.

[100] F.D. Cojocaru, D. Botezat, I. Gardikiotis, C.M. Uritu, G. Dodi, L. Trandafir, C. Rezus, E. Rezus, B.I. Tamba, C.T. Mihai, Nanomaterials designed for antiviral drug delivery transport across biological barriers, Pharmaceutics 12 (2020) 171.

[101] M. Chakravarty, A. Vora, Nanotechnology-based antiviral therapeutics, Drug Deliv. Transl. Res. (2020).

[102] N. Driscoll, A.G. Richardson, K. Maleski, B. Anasori, O. Adewole, P. Lelyukh, L. Escobedo, D.K. Cullen, T.H. Lucas, Y. Gogotsi, F. Vitale, Two-dimensional Ti_3C_2 MXene for high-resolution neural interfaces, ACS Nano 12 (2018) 10419–10429.

[103] B.B. Murphy, P.J. Mulcahey, N. Driscoll, A.G. Richardson, G.T. Robbins, N.V. Apollo, K. Maleski, T.H. Lucas, Y. Gogotsi, T. Dillingham, F. Vitale, A gel-free $Ti_3C_2T_x$ -based electrode array for high-density, high-resolution surface electromyography, Adv. Mater. Technol. 5 (2020) 2000325.

[104] F. Vitale, N. Driscoll, B. Murphy, Biomedical applications of MXenes, in: B. Anasori, Y. Gogotsi (Eds.), 2D Metal Carbides and Nitrides (MXenes): Structure, Properties and Applications, Springer International Publishing, Cham, 2019, pp. 503–524.

[105] R.P. Pandey, K. Rasool, V.E. Madhavan, B. Aïssa, Y. Gogotsi, K.A. Mahmoud, Ultrahigh-flux and fouling-resistant membranes based on layered silver/mxene ($Ti_3C_2T_x$) nanosheets, J. Mater. Chem. A 6 (2018) 3522–3533.

[106] G.C. Tremiliosi, L.G.P. Simoes, D.T. Minozzi, R.I. Santos, D.C.B. Vilela, E.L. Durigon, R.R.G. Machado, D.S. Medina, L.K. Ribeiro, I.L.V. Rosa, M. Assis, J. Andrés, E. Longo, L.H. Freitas-Junior, Ag nanoparticles-basedantimicrobial polycotton fabrics to prevent the transmission and spread of SARS-CoV-2, bioRxiv, 2020, 2020.2006.2026.152520.

[107] G. Pezzotti, E. Ohgitani, M. Shin-Ya, T. Adachi, E. Marin, F. Boschetto, W. Zhu, O. Mazda, Rapid inactivation of SARS-CoV-2 by silicon nitride, copper,and aluminum nitride, bioRxiv, 2020, 2020.2006.2019.159970.

[108] J. Hasan, A. Pyke, N. Nair, T. Yarlagadda, G. Will, K. Spann, P.K.D.V. Yarlagadda, Antiviral nanostructured surfaces reduce the viability of SARS-CoV-2, ACS Biomater. Sci. Eng. 6 (2020) 4858–4861.

[109] S.S. Jeremiah, K. Miyakawa, T. Morita, Y. Yamaoka, A. Ryo, Potent antiviral effect of silver nanoparticles on SARS-CoV-2, Biochem. Biophys. Res. Commun. 533 (2020) 195–200.

[110] Z. Zhong, S. Mc Cafferty, F. Combes, H. Huysmans, J. De Temmerman, A. Gitsels, D. Vanrompay, J. Portela Catani, N.N. Sanders, mRNA therapeutics deliver a hopeful message, Nano Today 23 (2018) 16–39.

[111] A. Puri, K. Loomis, B. Smith, J.-H. Lee, A. Yavlovich, E. Heldman, R. Blumenthal, Lipid-based nanoparticles as pharmaceutical drug carriers: from concepts to clinic, Crit. Rev. Ther. Drug Carrier Syst. 26 (2009) 523–580.

[112] S.C. Semple, A. Akinc, J. Chen, A.P. Sandhu, B.L. Mui, C.K. Cho, D.W.Y. Sah, D. Stebbing, E.J. Crosley, E. Yaworski, I.M. Hafez, J.R. Dorkin, J. Qin, K. Lam, K.G. Rajeev, K.F. Wong, L.B. Jeffs, L. Nechev, M.L. Eisenhardt, M. Jayaraman,

M. Kazem, M.A. Maier, M. Srinivasulu, M.J. Weinstein, Q. Chen, R. Alvarez, S.A. Barros, S. De, S.K. Klimuk, T. Borland, V. Kosovrasti, W.L. Cantley, Y.K. Tam, M. Manoharan, M.A. Ciufolini, M.A. Tracy, A. de Fougerolles, I. MacLachlan, P.R. Cullis, T.D. Madden, M.J. Hope, Rational design of cationic lipids for sirna delivery, Nat. Biotechnol. 28 (2010) 172–176.

[113] U. Sahin, K. Karikó, Ö. Türeci, mRNA-based therapeutics — developing a new class of drugs, Nat. Rev. Drug Discov. 13 (2014) 759–780.

[114] M. Seredych, B. Haines, V. Sokolova, P. Cheung, F. Meng, L. Stone, L. Mikhalovska, S. Mikhalovsky, V.N. Mochalin, Y. Gogotsi, Graphene-based materials for the fast removal of cytokines from blood plasma, ACS Appl. Bio Mater. 1 (2018) 436–443.